2015 年 2 月
碩士學位 論文

Surface Characteristics of Hydroxyapatite Film on the Micro-pore Structured Ti-35Ta-xNb Alloys by Electrochemical Deposition Method

朝 鮮 大 學 校 大 學 院

光 技 術 工 學 科 (光 應 用 工 學 專 攻)

趙 采 翼

Surface Characteristics of Hydroxyapatite Film on the Micro-pore Structured Ti-35Ta-xNb Alloys by Electrochemical Deposition Method

전기화학적 석출법으로 마이크로 포어구조를 형성한
Ti-35Ta-xNb 합금의
수산화인회석 피막의 표면특성

2015年 2月 25日

朝 鮮 大 學 校 大 學 院

光 技 術 工 學 科 (光 應 用 工 學 傳 攻)

趙 采 翼

Surface Characteristics of Hydroxyapatite Film on the Micro-pore Structured Ti-35Ta-xNb Alloys by Electrochemical Deposition Method

指導教授　崔 漢 喆

이 論文을 工學 碩士學位申請 論文으로 提出함

2014年　10月

朝 鮮 大 學 校　大學 院

光 技 術 工 學 科 (光 應 用 工 學 專 攻)

趙 采 翼

趙采翼의 碩士學位論文을 認准함

委 員 張 朝鮮大學校 敎 授 金 炳 勳 印

委 員 朝鮮大學校 敎 授 安 相 建 印

委 員 朝鮮大學校 敎 授 崔 漢 喆 印

2014年 11月

朝 鮮 大 學 校 大 學 院

CONTENTS

LIST OF TABLES

LIST OF FIGURES

국 문 초 록

전기화학적 석출법으로 마이크로 포어구조를 형성한 Ti-35Ta-xNb 합금의 수산화인회석 피막의 표면특성

조 채 익
지도교수: 최한철, 공학박사
광기술공학과(광응용공학전공)
조선대학교 대학원

생체재료로 사용되고 있는 티타늄 및 티타늄합금은 생체비활성재료로서 높은 강도와 우수한 내식성을 가지고 있어 정형외과 재료로서 널리 사용되고 있다. 하지만 현재 임플란트에서 가장 많이 사용되고 있는 Ti-6Al-4V 합금은 합금의 원소인 알루미늄과 바나듐의 신체에 유해한 작용을 줄 우려가 있어 본 연구에서는 나이오븀, 탄탈륨, 하프늄 등의 원소를 첨가하여 새로운 티타늄 합금을 제조한 후 표면에 마이크로포아를 형성한 후, 그 표면에 수산회인회석을 석출하여 표면특성을 조사하였다. Ti-35Ta-xNb 삼원계 합금은 Ti-35Ta 이원계 합금을 기반으로 하여 나이오븀의 함량을 0, 5, 10, 및 15 wt. %의 함유량으로 정량을 한 후 아크용해법을 이용하여 실시하였다. 제조된 합금은 1000 ℃에서 12시간 동안 열처리를 실시한 후 0 ℃ 수냉을 실시하였다. 표면에 마이크로포어를 형성함과 동시에 수산화인회석의 코팅막의 결합력을 증진시키기 위해 0.15 M 칼슘포스페이트 모노하이드라이트 (Calcium acetate monohydrate) + 0.02 M 칼슘 글리세로포스페이트 (Calcium glycerophosphate)를 280 V에서 3분 간 DC power supply를 이용하여 인가를 하였다. 표면내식성 테스트는 동전위 분극시험을 통하여 분석을 하였다.
이러한 실험을 통하여 다음과 같은 결론을 얻었다.

1. 양극산화법을 이용한 마이크로 포어의 형성은 전압이 증가할수록 포어의 크기가 증가하였으며, 나이오븀의 함유량이 증가할수록 포어의 크기가 작아졌다.
2. 나이오븀을 첨가하였을 경우 침상구조에서 등축정구조로 변함을 확인할 수 있었으며, 이는 상 분석을 실시한 결과 베타상이 증가하면서 생긴 현상임을 확인할 수 있었다.
3. 나이오븀의 함유량이 증가할수록 내식성이 증가하였으며 300 ㎷에서의 전류밀도값은 산화막을 형성하였을 경우 더욱 좋아졌으며, 나이오븀을 첨가할수록 내식성이 증가하였다.

결론적으로, 마이크로 포어를 형성한 후 수산화인회석을 코팅한 Ti-35Ta-xNb합금은 골형성을 유도할 수 있는 수산화인회석과 세포증식이 용이한 환경을 제공할 것으로 사료되며, 높은 내식성도 가지고 있어 생체재료로서 응용이 가능함을 알 수 있었다.

Ⅰ. INTRODUCTION

Dental materials have been successfully used for a variety of biomaterial, and different designs, commercial pure titanium (Cp-Ti), Ti-6Al-4V alloy, nickel-titanium shape memory alloys are widely used for dental materials due to offers several benefits, excellent corrosion resistance and enhanced biocompatibility [1-3]. Especially, Ti-6Al-4V is the most widely used material due to its excellent strength, good corrosion resistance in clinical use. However, Ti-6Al-4V alloy has properties of high elastic modulus when compared with that of bone and potential adverse human effects[4, 5]. For this reason, new β type Ti alloys are composed of non-toxic elements such as Nb, Ta, Zr, Hf, Mo and Sn due to lower elastic modulus, excellent corrosion resistance and enhanced biocompatibility. Especially, Ta and Nb can reduce the modulus of elasticity when alloyed with Ti due to β-stabilizer [4, 6, 7]. To enhanced biocompatibility, surface treatment on Ti alloys were widely used for biomaterial such as pulsed laser deposition, plasma spray, magnetron sputtering, alkali treatment, electron-beem physical vapor deposition, and electrochemical deposition [8-13]. Especially, electrochemical anodic oxidation is known as excellent method in the biocompatibility of biomaterial due to quickly coating time and controlled coating condition.[16] The anodizing oxide layer and diameter modulation of Ti alloys can be obtained function of improvement of cell adhesion [14, 15]. Hydroxyapatite (HA; $Ca_{10}(PO_4)_6(OH)_2$) was widely known as being osteo-conductive, and was able to promote bone in-growth and attachment to the surface of the implant during the early stages of the implantation [16, 17]. Some of studies have been developed for HA coatings with good mechanical properties on Ti alloys for dental implant application. An ideal HA coating is expected to be fully dense and to have a good adhesion at the coating with Ti interface to minimize Ti-body fluid contact [18].

In this study, we investigated the surface characteristics of hydroxyapatite film on the micro-pore structured Ti-35Ta-xNb alloys by electrochemical deposition method.

II. BACKGROUND

2.1 Titanium [19]

The Ti is found in Reverend William Gregor in 1798. Because of titanium exist in a constituent of practically all crystalline rock and its high reactivity, Ti has not become more widely used until the latter half of the twentieth century [19]. For this reason, Ti has difficulty getting pure Ti and even now Ti is still very expensive compared with, for example, stainless steel. Fig. 1 shows transformations of Ti. Basically, Ti and Ti-based alloys can classified into α type (HCP : hexagonal-closed packed crystalline structure), near α type, (α+β type, and β type (BCC: body-centered cubic crystalline structure) alloy groups. Alloying elements added to Ti were divided into two groups: α stabilizers and (either singly of C, O, and N or in combination), dissolve into the Ti matrix and are strong solid solution strengthener which produce little change at the transformation temperature (β-transus: 883 ℃ for pure Ti) from the HCP to the BCC structure of pure Ti when heating and from the BCC to HCP when cooling [19-21].

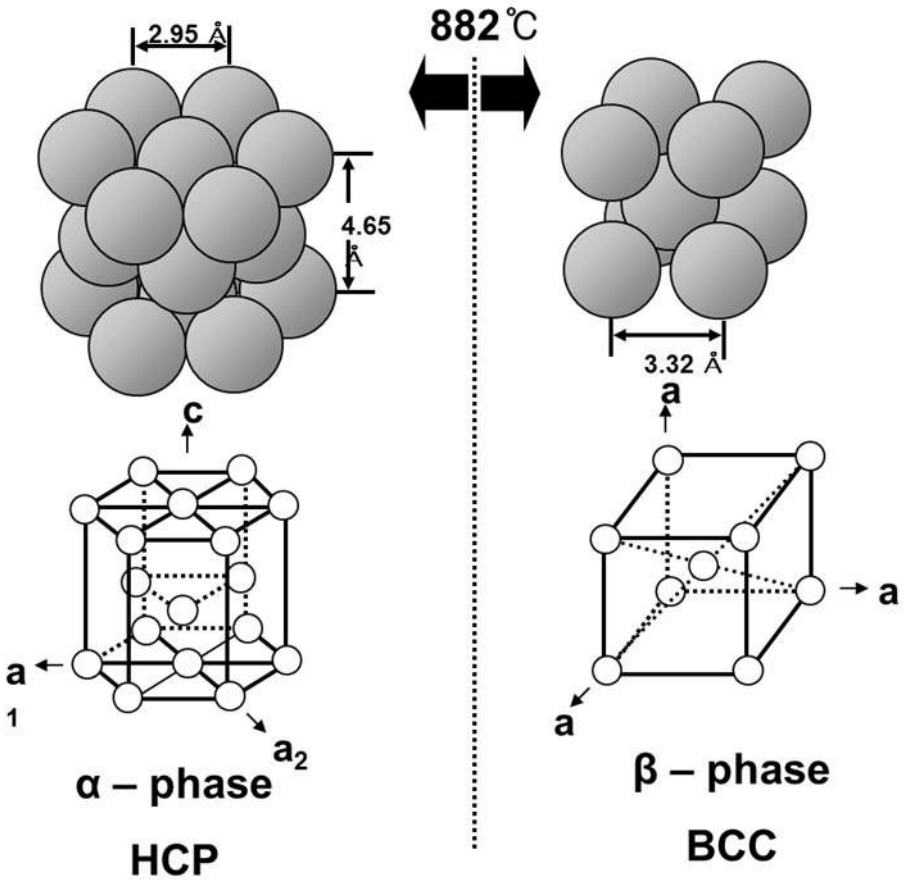

Fig. 1. Allotropic transformation of Ti [22].

2.1.1 Cp-Ti [23]

Cp-Ti is a white, lustrous metal which has the attraction of low density, good ductility and constitutes an important alloying element with many other metals. Alloys of Ti are widely used in the aircraft industry and have military applications because of their light weight, strength and ability to withstand high temperatures. Under the category of 'unalloyed grades' of ASTM specification, there are five materials classified in this group; they include ASTM grade 1 (99.5% Ti), grade 2 (99.3% Ti), grade3 (99.2% Ti), grade 4 (99.0% Ti).

- Grade 1 : grade 1 Cp Ti is the lowest strength unalloyed Ti with a sightly lower residual content. Both oxygen and iron residuals improve the impact strength. Oxygen acts as an interstitial strengthener, maintaining a single α phase HCP microstructure. Iron acts as a second β phase BCC grain refiner, offering moderate strengthening capabilities. The lower residual content makes grade 1 the lowest strength Cp Ti.
- Grade 2 : grade 2 is the most frequently selected Ti grade in industrial service having well-balanced properties of both strength and ductility. The strength levels are very similar to those of common stainless steel and its ductility allows for good cold formability.
- Grade 3 : Cp Ti grade 3 possesses a slightly higher strength due to its slightly higher residual content (primarily oxygen and also nitrogen) with slightly lower ductility.
- Grade 4 : grade 4 is the highest strength grade of the Cp Ti series; it serves mainly in the aerospace/aircraft industry [23, 24].

2.1.2 Ti-6Al-4V alloy [25]

Ti-6Al-4V alloy is widely used for dental materials due to their excellent biocompatibility and good mechanical properties. The Ti-6Al-4V, is a promising clinical implant material because the alloy has higher fatigue

strength compared to pure Ti [25]. This alloy belongs to the α + β phase alloy group and is particularly popular because of its high corrosion resistance and the reputed low toxicity of ions released from the surface due to dense and protective passive oxide (which is mainly TiO_2) film formation. Ti-6Al-4V (which is, in some articles, marked as Ti-6/4) exhibits good mechanical and excellent tissue compatibility properties that make it well suited for biomedical applications where a bone anchorage is required, particularly for implant applications. Ti-6Al-4V ELI is also available and employed in the medical area. When aluminium(Al) and vanadium(V) are added to Ti in only small quantities the strength of the alloy is much increased over that of Cp-Ti. Al is considered to be an α stabilizer and with V acting as a β stabilizer, the temperature at which the α to β transition occurs is depressed such that both the α and β forms can exist at room temperature. For the Ti-6A1-4V alloy considerably higher tensile properties [26] are achievable than for pure Ti which makes it attractive for use in high stress-bearing situations, such as the hip prosthesis and artificial knee joint. Nevertheless Cp-Ti is widely used for dental implants and so far the lower strength has not proved to be a problem.

2.1.3 Ti-Ta alloy system [27]

An interesting study was dine by Breme et al [27]. is used isoelastic porous sintered Ti-30Ta alloy and Ti wire loop ti accomplish the mechanical compatibility in endosseous dental implant systems. Their mechanical properties were optimized by the production parameter such as sintering and DB. The functionality was tested after insertion into an artificial jaw which had properties corresponding to the natural mandibular. It was reported that the elastic properties of both implants are similar to the properties of the bone, and the implant has a safe severe plastic deformation was investigated [28].

2.1.4 Ti-Nb alloy system [29]

Ti-Nb alloys have been shape memory alloy (SMA) characteristics at room temperature, and their SMA properties can be considerably improved by thermo mechanical treatment. Because Ti-Nb alloy has metastable β Ti alloy and solution treated it, followed by aging at 482 ℃. Especially, Ti-35Nb-7Zr-5Ta alloys exhibited 0.2 % off set yield strength of 1,300 MPa with 8 % elongation, due to ω + β and ω + α + β phase precipitation and this enhanced strength makes the alloy a candidate for bone plates and screw [29].

2.1.5 α and β Ti alloys [31]

The α to β transformation temperature of pure Ti either increases or decreases based on the nature of the alloying elements. Table 1 shows element of α and β stabilization. The alloying elements such as (Al, O, N, etc.) that tend to stabilize the α phase are called α stabilizers and the addition of these elements increase the β transus temperature, while elements that stabilize β phase are known as β stabilizers (V, Mo, Nb, Fe, Cr, etc.) and addition of these elements depress the β transus temperature [30]. The basic design of the alloys is the substitution of and Al with Nb, Ta, Zr and Hf, which are in groups 4 and 5 in the periodic table 1. On the other hand, β phase show a low Young's modulus and may prevent street shielding as used for bone fixtures [31].

Table 1 Elements of α and β stabilization [31]

Element	Type	Element	Type	Element	Type	Element	Type
V	β-Isomorphous	Mn	β-Eutectoid	Ag	β-Eutectoid	Sn	Neutral/β-Iso
Nb	β-Isomorphous	Fe	β-Eutectoid	W	β-Eutectoid	Al	α
Mo	β-Isomorphous	Co	β-Eutectoid	Pt	β-Eutectoid	O	α
Ta	β-Isomorphous	Ni	β-Eutectoid	Au	β-Eutectoid	N	α
Re	β-Isomorphous	Cu	β-Eutectoid	Hf	Neutral/β-Iso		
Cr	β-Eutectoid	Pd	β-Eutectoid	Zr	Neutral/β-Iso		

2.1.6 β Ti alloys [31]

Most β Ti alloys contain small amounts of α stabilizers which permit second phase strengthening to high levels at room to moderate temperatures. The BCC β phase is ductile, and therefore β Ti alloys are easily cold formation. The β alloys are prone to ductile to brittle transformation, and thus are not used for cryogenic applications. The major alloying elements for β alloys elements of Mo, Nb and Ta are also the elements that are considered to be very biocompatible, more so than the α stabilizing elements like Al and Ti.

The β alloys may be strengthened by the solid solution effect of the β stabilizer additions, but large strength increases also result from small volume (typically <5%) second phase precipitation during heat treatment. Because of attractive hot and cold workability properties, much effort has been devoted to creating specialized β Ti alloys for specific applications. Even though the interest in, and the manufacture of, β Ti grades is growing, the total worldwide output of Ti mill products includes only a few percent of β Ti alloys by weight [31].

2.2 Ceramic [32]

Calcium phosphates (CaP) are the most common family of bioceramics well known for their use in biological applications. Table 2 shows various calcium phosphate according to Ca/P ratio. They belong to the family of biocompatible apatites and there are several CaP phases, the most common being HA. Other structures include brushite (DCPD; $CaHPO_4 \cdot 2\ H_2O$) and tricalcium phosphate (TCP; $Ca_3(PO_4)_2$). At the physiological pH of 7.2-7.6 HA is most stable of all the calcium phosphates. Therefore, HA has attracted attention of biomaterial researchers. Several low and high temperature approaches have been reported for synthesizing HA and brushite while TCP is synthesized primarily using high temperature methods [32]. Characteristics of these three CaP phases are given below.

Table 2 Main calcium phosphate (CaP) [33]

Name	Symbol(s)	Formula	Ca/P
Monocalcium phosphate monohydrate	(MCPM) and (MCPH)	$Ca(H_2PO_4)_2 \cdot H_2O$	0.5
Monocalcium phosphate anhydrous	(MCPA) and (MCP)	$Ca(H_2PO_4)_2$	0.5
Dicalcium phosphate dihydrate (Brushite)	(DCPD)	$CaHPO_4 \cdot 2H_2O$	1
Dicalcium phosphate anhydrous (Monetite)	(DCPA) and (DCP)	$CaHPO_4$	1
Octacalcium phosphate	(OCP)	$Ca_8(HPO_4)_2(PO_4)_4 \cdot 5H_2O$	1.33
α-Tricalcium phosphate	(α-TCP)	$Ca_3(PO_4)_2$	1.5
β-Tricalcium phosphate	(β-TCP)	$Ca_3(PO_4)_2$	1.5
Amorphous calcium phosphate	(ACP)	$Ca_x(PO_4)_y \cdot nH_2O$	1.2-2.2
Hydroxyapatite	(HA) and (HAp)	$Ca_{10}(PO_4)_6(OH)_2$	1.67

2.2.1 Hydroxyapatite [38]

Biomaterials are used to replace parts of a living system or to function in intimate contact with living tissue. Fig. 2 shows structure of bone in the size of macro scale to nano scale. Especially, the nano scale is composed by collagen molecular and HA crystal. They are intended to restore, replace, or treat any tissue, organ, or function of the body. HA is similarity to the mineral part of bone [34]. Calcium phosphate is usually carbonated HA with a Ca/P ratio of less than 1.67. The HA has been of interest owing to its excellent biocompatibility [35], affinity to biopolymers and high osteogenic potential [36]. Because It has been well documented that HA can promote new bone ingrowth through osteo-conduction mechanism without causing any local or systemic toxicity, inflammation or foreign body response [37]. When a HA based ceramic is implanted, a fibrous tissue-free layer containing carbonated apatite forms on its surfaces and contributes to the bonding of the implant to the living bone, resulting in earlier implant stabilization and superior fixation of the implant to the surrounding tissues [38].

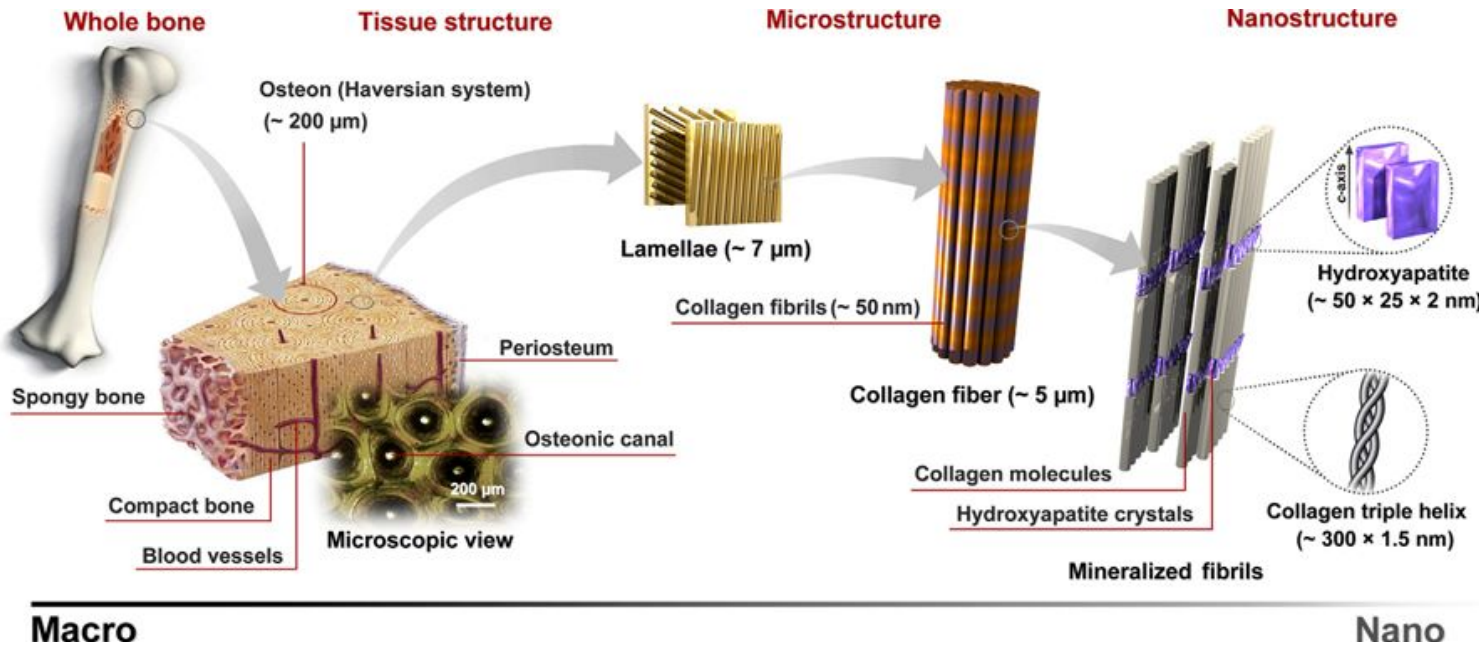

Fig. 2. The hierarchical structure of typical bone at various length scales [38].

2.2.2 Surface modification techniques [39]

In Table 3, surface modification techniques are categorized according to their processes and purposes. Major purpose of surface modification is to improve hard tissue compatibility or accelerate bone formation. Research to improve hard tissue compatibility involves two approaches based on the resultant surface layer: a calcium phosphate and Ti oxide layer with the thickness measured in micrometers and a surface-modified layer with the thickness measured in nanometers. Most of these processes have been developed since the 1990s. Fig. 3 shows the history of the surface treatment technique to improve hard tissue compatibility. Surface property is particularly significant for biomaterials, and thus surface modification techniques are particularly useful to biomaterials. Dry process (using ion beam) and wet process (which is performed in aqueous solutions) are predominant surface modification techniques. In particular, electrochemical technique in the wet process is important near recently. Immobilization of bone formation factors such as bone morphological protein, BMP, or biomolecules such as collagen and peptide to metal surface is another technique to improve hard tissue compatibility. On the other hand, the immobilization of biofunctional molecules such as poly(ethylene glycol), PEG, to the metal surface to control the adsorption of proteins and adhesion of cells, platelets, and bacteria is attempted.

Table 3 Categorization of surface treatment techniques of metals for medical devices according to the process and purpose [39]

	Dry process	Electrochemical process Micro-arc oxidation	Chemical and Hydrothermal process
Hydroxyapatite or calcium phosphate coating	Commercialized	Commercialized	Studied
TiO_2 or $CaTiO_3$ coating	Commercialized	Commercialized	
Surface-modified layer formation			Commercialized
Immobilization of functional molecules and biomolecules		Studied	Studied

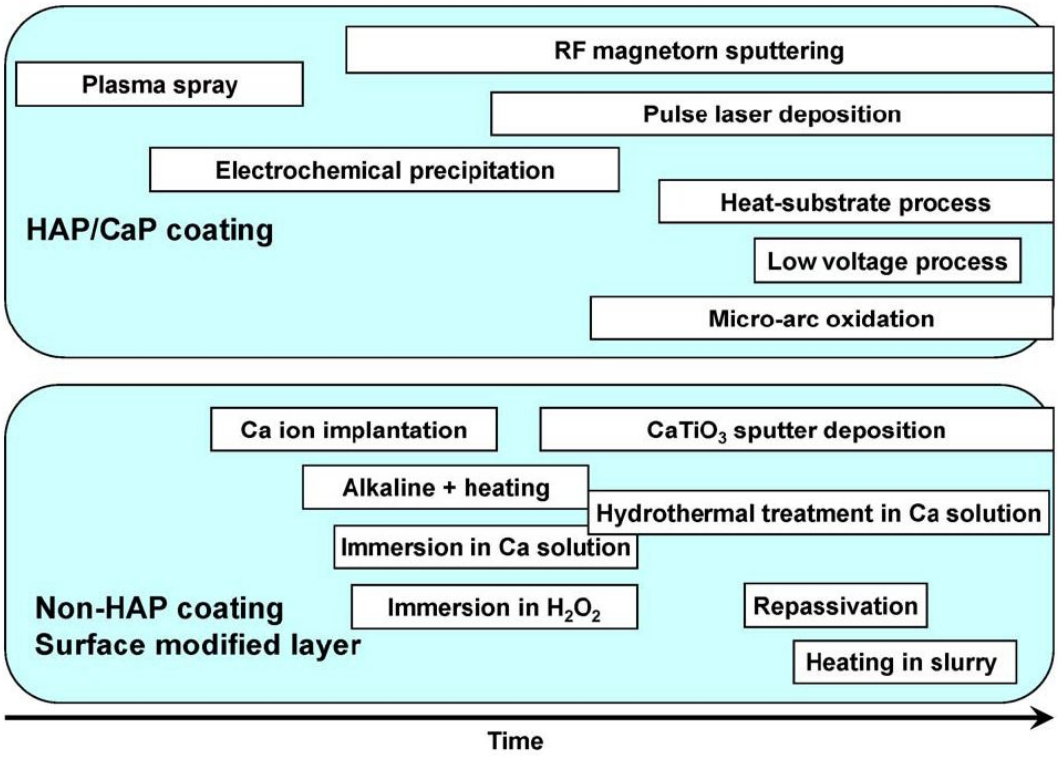

Fig. 3. History of surface treatment technique to improve hard tissue compatibility. Approaches to improving hard tissue compatibility are categorized based on the resultant surface layer: calcium phosphate layer formation with thickness measured in micrometers and surface-modified layer formation with thickness measured in nanometers [39].

2.2.3 Micro-pore oxidation [39]

Micro-pore oxidation is a relatively convenient technique for forming oxide layer on metals. Fig. 4 shows surface of micro-pore structured Ti-35Ta alloy. It is effective for the formation of porous or irregular-shaped TiO_2 layer on Ti substrate and Ta_2O_5 layer on Ta substrate. The advantage of micro-pore oxidation is that coating layer is not only porous but also uniformly coated on metal surfaces with complex geometry. Anodically electrochemical deposition and micro-pore oxidation are not clearly distinguished. In the case of the formation of an oxide layer with connecting pore to the substrate metal by high voltage, this technique is usually categorized as micro-pore oxidation. In this sense, some of the electrochemical techniques explained above belong to micro-pore oxidation. Micro-pore oxidation is currently used to obtain thick and porous oxide or HA layer [39-43]. Ultraviolet irradiation of micro-pore oxidation coating in distilled water enhances bioactivity. This technique is also applied to Ta.

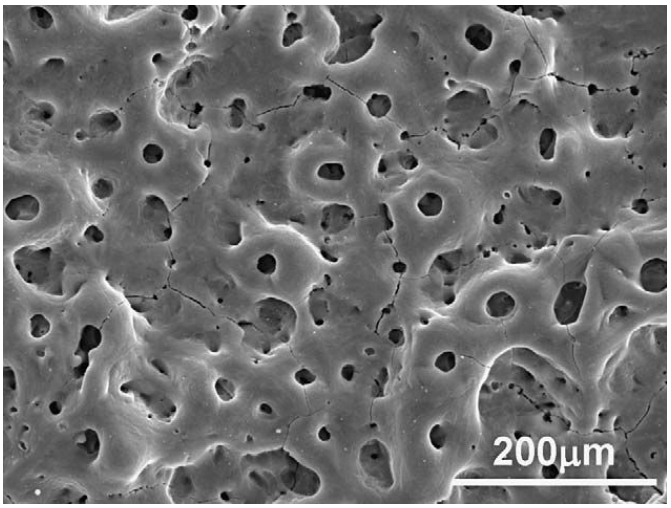

Fig. 4. FE-SEM images of micro-pore structured Ti-35Ta at 270 V in 0.15 M Calcium monohydrite + 0.02 M Calcium glycerophosphate at 3 min [39].

2.2.4 HA coating [55]

Electrochemical treatment is used commonly to form an HA layer on Ti [44]. The carbonate-containing HA with a desirable morphology such as plate, needle, and particle could be precipitated on a Ti substrate, it is advantages of be bone growth and penetration depth, with a more direct contact between the tissue and the implant surface[45,46]. The β-TCP is coated on Ti for immobilization of collagen [47]. Low-voltage alternating current is also effective to precipitate calcium phosphate on Ti [48]. This technique is useful for the treatment of thin wire and fiber without the dissolution of Ti. The HA coating method is used for enhance biocompatibility such as immersion, sol-gel, plasma spray, sputtering and electrochemical deposition [49]. Especially, electrochemical deposition method is adjusted to thickness and pore size [50]. Nano-grained calcium phosphate is electrochemically deposited on Ti using acidic electrolytes [51]. The coating layer contains dicalcium phosphate dihydrate (55-85 nm in grain size) with a small amount of HA (20-25 nm); the content of HA increases with the increase of the current density [52]. An electrochemical method of producing nanocrystalline HA coatings on Ti surface is reported [53,54]. Also, HA is coated by dynamic voltage during electrophoretic deposition [55].

III. MATERIALS AND METHODS

3.1. Preparation of Ti-35Ta-xNb alloys

The Ti-35Ta-xNb alloys, with Nb contents ranging from 0 and 10 wt. % were prepared using CP-Ti (G&S Ti, Grade 4, USA), Nb (Kurt J. Lesker Company, 99.95 wt.% purity, USA) and Ta (Kurt J. Lesker Company, 99.95 wt.% purity, USA). The Ti-35Ta-xNb alloys were manufactured from the component metals, using a vacuum arc-melting furnace (SVT, KOREA) with a water-cooled copper hearth and a high-purity Ar atmosphere. The Ti-35Ta-xNb ingots were remelted at least six times in order to avoid inhomogeneity. The ingots of Ti-35Ta-xNb alloy were obtained in the form of rod with about length of 60 mm and diameter of 10 mm, and ingots were approximately 20 g in weight. The ingots of Ti-35Ta-xNb alloy were homogenized in Ar atmosphere at 1000 ℃ (MSTF-1650, MS Eng, KOREA) for 12 h followed by 0 ℃ water quenching. To manufacture the cylindrical specimens with diameter of 10 mm and thickness of 3 mm), ingots were cut off by diamond wheel cutting system (Accutom-5, Struers, Denmark). The sample was polished by standard ANSI silicon carbide papers of different grades ranging from 100 to 2000 and finally alumina (1 μm) polished, ultrasonically cleaned in deionized water and dried in flowing nitrogen.

3.2. Analysis of surface characteristics for Ti-35Ta-xNb alloys

The phase and composition of the Ti-35Ta-xNb alloys were determined by using an X-ray diffractometer (XRD, X`pert PRO, Philips). Ni-filtered Cu K_{α} radiation was used in this study. Phase was identified by matching each characteristic peak with JCPDS files. The Ti-35Ta-xNb alloys, micro-pore and hydroxyapatite coating surfaces were observed by optical microscopy (OM, olympus, BX 60M, Japan), field-emission scanning electron microscopy (FE-SEM, Hitachi, 4800, Japan) and energy dispersive x-ray analysis (EDX, Oxford ISIS 310, England). The etching treatment was performed in Keller's reagent with 2 ml HF, 3 ml HCl, 5 ml HNO_3, and 190 ml H_2O.

3.3. Micro-pore formation on the Ti alloy surface

The electrochemical experiment consisted of a two electrode configuration with platinum. The electrolyte used was 0.15 M Calcium acetate monohydrate + 0.02 M Calcium glycerophospate at room temperature. The electrochemical anodization was carried out at constant voltage (280 V) for 3 min (KDP-1500, KOREA).

3.4. Electrochemical deposition

Precipitation of HA is performed on the alumina polished and micro-pore treated Ti-35Ta-xNb alloy surfaces using a potentiostat (PARSTAT 2273, Princeton Applied Research, USA). The electrochemical setup for HA deposition consisted of a three-electrode configuration with a carbon electrode and a saturated calomel electrode (SCE) as the counter electrode and reference electrode, respectively. The electrolyte for HA deposition was composed of 2.5 mM $Ca(NO_3)_2$ ·4 H_2O + 1.5 mM $NH_4H_2PO_4$ in distilled water; the Ca/P ratio for the electrolyte was 1.67. A single voltammetry cycle was composed of a 2 s deposition time with potential E ranging from -1.5 V to 0.3 V (vs. SCE electrode) and scan rate of 500 mV/s, followed by a break time of 2 s. The number of cycles employed for this electrochemical HA deposition, performed at 80 ° C. Overall analysis is summarized in Table 4.

Table 4 The conditions of electrochemical deposition

	Electrochemical deposition
Working equipment	EG&G Co, Model: PARSTAT 2273
Working electrode	Samples (Ti-35Ta-xNb alloys)
Reference electrode	SCE
Counter electrode	High dense carbon
electrolyte	2.5 mM $Ca(NO_3)_2$·4 H_2O + 1.5 mM $NH_4H_2PO_4$
Working temperature	80 ± 1 ℃
deposition time	2 second
Scan rate	500 mV/sec
Scan definition	- 1500 mV ~ + 300 mV
cycle	5, 30, 50 cycles

3.5 Morphology observation of surface treatment on the Ti-35Ta-xNb alloys

The morphology of the porous titanium oxide and HA film on Ti-35Ta-xNb alloys characterized by a field-emission scanning electron microscopy (FE-SEM, Hitachi S-4800, Japan) and X-ray diffractometer (XRD, X`pert PRO, Philips).

3.6. Corrosion test for Ti-35Ta-xNb alloys

Corrosion behaviors were investigated using a standard three-electrode cell having the specimen as a working electrode and a high dense carbon counter electrode. The potential of the working electrode was measured against a saturated calomel electrode (SCE) and all specimen potentials were referenced to this electrode. The corrosion properties of the specimens were first examined by a potentiodynamic polarization test (potential range from -1500 to 2000 mV) at scan rate of 1.67 mV/s in 0.9 % NaCl solution at 36.5 ± 1 ℃. (PARSTAT 2273, EG&G Company, USA). Using an automatic data acquisition system, the potentiodynamic polarization curves were plotted and both corrosion rate and potential were estimated by Tafel plots by using both anodic and cathodic branches. The condition of electrochemical corrosion test were shown in Table 5.

Table 5 The conditions of electrochemical corrosion test

	Potentiodynamic test
Working equipment	EG&G Co, Model:PARSTAT 263A
Working electrode	Samples (Ti-35Ta-xNb alloys)
Reference electrode	SCE
Counter elctrode	High dense carbon
electrolyte	0.9 % NaCl
Working temperature	36.5 ± 1 ℃
Gas purging	Ar gas, 10 minute
Scan rate	100 mV/min
Scan definition	- 1500 ~ + 2000 mV

IV. RESULTS AND DISCUSSION

4.1. Microstructure of Ti-35Ta-xNb alloys

Fig. 5 shows the microstructure of the Ti-35Ta-xNb alloys with different Nb content (0 and 10 wt. %) after heat treatment at 1000 ℃ for 12 h in Ar atmosphere, followed by 0 ℃ water quenching. For Ti-35Ta alloy is observed needle-like α phase, which can be seen in Figure 5(a) and (b). The needle-like also is observed at Ti-35Ta-10Nb alloy in Fig. 5(c) and (d) but this microstructure has more equiaxed β phase. It is considered that needle-like martensite plates were transformed to equiaxed β phase with in Nb content and homogenization treatment at 1,000 ℃ in 12 h followed by ice water quenching. The elements of Ta and Nb is stabilized β phase [56-58]. For more accurate analysis, Ti-35Ta-xNb alloys is carried out XRD analysis in range of 0 to 80 degree. Fig. 6 shows the peaks on the XRD patterns of homogenized Ti-35Ta-xNb alloys. The peaks of Ti-35Ta-xNb alloys are check using JCPDS card data for element standards. The peak intensity of Ti-35Ta-10Nb alloys showed higher β phase with increment of Nb content, whereas, that of α" phase decreased. And Ti-35Ta-xNb alloys showed homogeneous crystal structure by quenching. It confirmed that Nb contents to Ti alloy plays role in increasing the β phase with equiaxed structure by stabilized β phase [56]. In addition, element of Ta has influence on formation of hexagonal martensite and orthorhombic martensite. It is assumed that this alloy has law elastic modulus and can be appled bone materials [59].

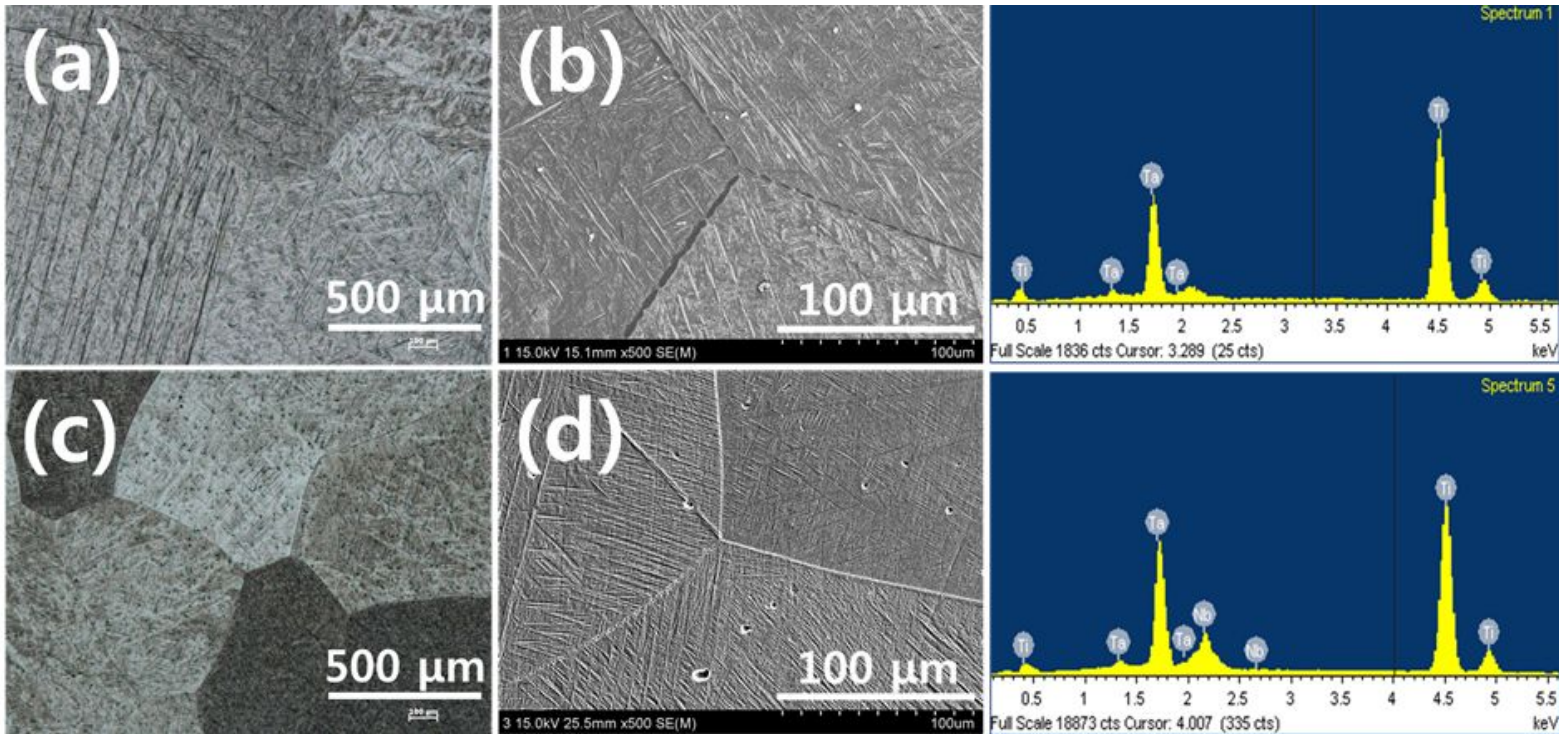

Fig. 5. OM, FE-SEM images and EDS analysis of Ti-35Ta-xNb alloys after heat treatment at 1000 ℃ for 12 h in Ar atmosphere, followed by 0 ℃ water quenching: (a) OM images of Ti-35Ta (b) FE-SEM images of Ti-35Ta (c) OM images of Ti-35Ta-10Nb (d) FE-SEM images of Ti-35Ta-10Nb.

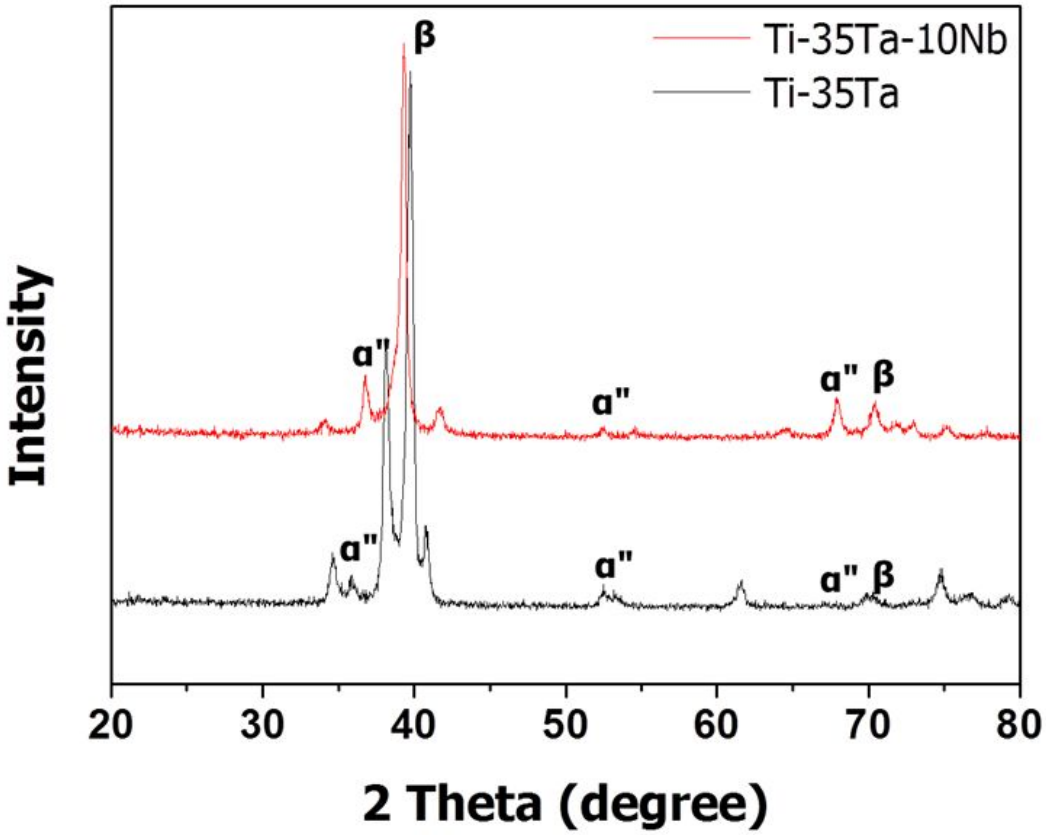

Fig. 6. XRD patterns of Ti-35Ta-xNb alloys after heat treatment at 1000 ℃ for 12 h in Ar atmosphere, followed by 0 ℃ water quenching.

4.2. The micro-pore surface morphology of Ti-35Ta-xNb alloys

Fig. 7 shows the XRD patterns of Ti-35Ta-xNb alloys by anodization in 0.15 M calcium acetate monohydrate + 0.02 M calcium glycerophospate at 240 V to 320 V for 3 min. The spark shows at approximately 170 V, the XRD peaks of 240 V shows broad line. The XRD peaks of 280 V is observed rutile peak, the peaks of 320 V is observed rutile peak and anatase peak. Especially, the more voltage is increased, the more intensity is increased. The reason that occurrences of spark at 170 V is spark discharge surface due to insulation breakdown of the surface [60, 61]. Also through Fig. 7, the more voltage is increased, the more micro-pore barrier layer is increased. The fractions of rutile in the anodic oxides were calculated using the following equation [62].

$$f_{rutile} = 0.679 \cdot (I_{rutile} / \{I_{rutile} + I_{anatase}\}) + 0.312 \cdot (I_{rutile} / \{I_{rutile} + I_{anatase}\})^2$$

Analysis of f_{rutile}, the values of f_{rutile} are as shown in Table 6. The more voltage is increased, the more values of f_{rutile} are increased. Fig. 8 shows FE-SEM images of micro-pore formed on Ti-35Ta-10Nb alloys in 0.15 M Calcium acetate monohydrate + 0.02 M Calcium glycerophospate. The pore size is increased as the voltage increased, it is confirmed that pores are formed as a whole. This result is associated with Fig. 7 XRD analysis data. Therefore, The more voltage is increased, The more pore size and thickness of barrier layer is increased [63].

Table 6 Voltage values of rutile

	I_{rutile}	$I_{anatase}$	f_{rutile}
240 V	20	37	0.278
280 V	30	47	0.313
320 V	173	245	0.336

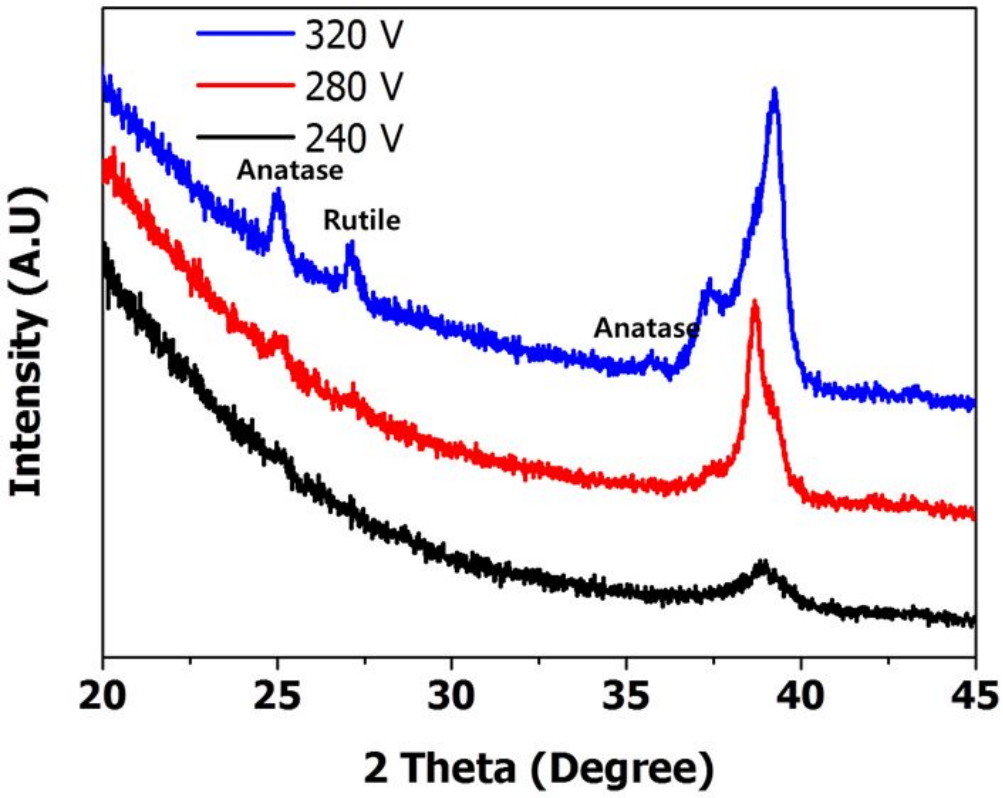

Fig. 7. XRD patterns of Ti-35Ta-10Nb alloys with variation of applied voltages in 0.15 M calcium acetate monohydrate + 0.02 M calcium glycerophospate from 240 V to 320 V for 3 min.

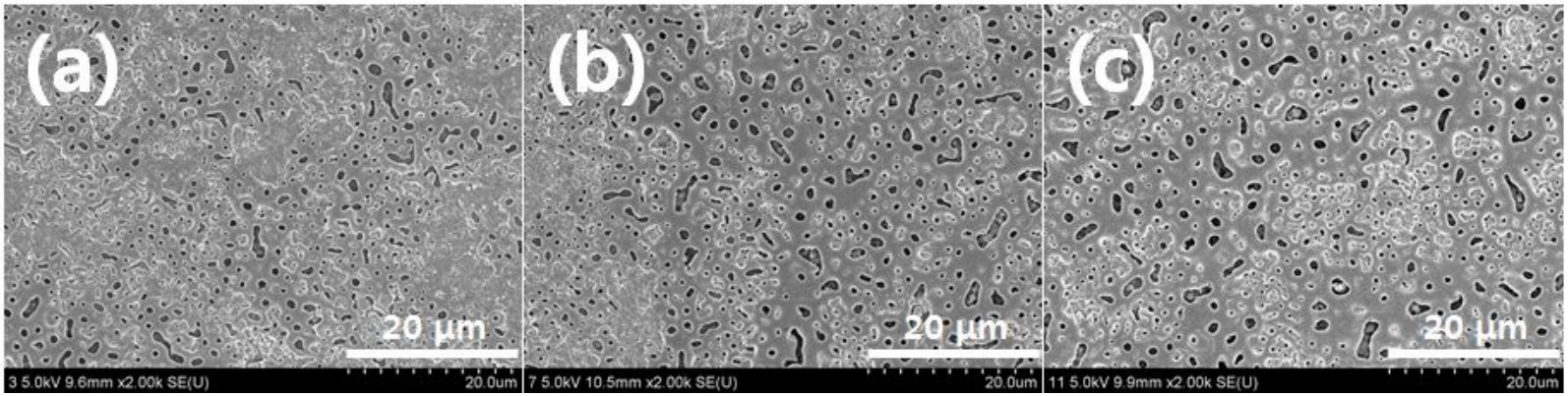

Fig. 8. FE-SEM images of micro-pore formed on Ti-35Ta-10Nb alloys in 0.15 M calcium acetate monohydrate + 0.02 M calcium glycerophospate ; (a) 240 V, (b) 280 V, (c) 320 V.

Fig. 9 shows the FE-SEM images of micro-pore formed on Ti-35Ta-xNb alloys by anodization in 0.15 M Calcium acetate monohydrate + 0.02 M Calcium glycerophospate at 280V for 3 min. The Fig. 9(a) and Fig. 9(c) show bare micro-pore surfaces of Ti-35Ta-xNb alloys at 280 V for 3 min, the Fig. 9(b) and Fig. 9(d) show NaOH treated micro-pore surfaces of Ti-35Ta-xNb alloys at 280 V for 3 min. The process of NaOH treatment is performed in 5 M NaOH solution at for 10 min. It is conformed that more rough micro-pore surface showed in the case of NaOH treated Ti-35Ta-xNb alloys. From the investigate the micro-pore structure, it has been observed in micro-pore inside of pore in the case of NaOH treatment as shown in Fig. 10. it is confirmed that nano-sized network structure was formed. The surface of nano-sized network structure was known as $Na_5Ti_5O_{11}$ and $Na_2Ti_6O_{13}$ [64]. In case of similar coating, calcium phosphate film was immersed in SBF solution after alkali treatment [65]. In case of biomaterial, the sizes of network structure and micro-pore can be used for good biological materials, that is, this structure has advantage with cell culture due to provide a good cell environment and to increased surface area[66].

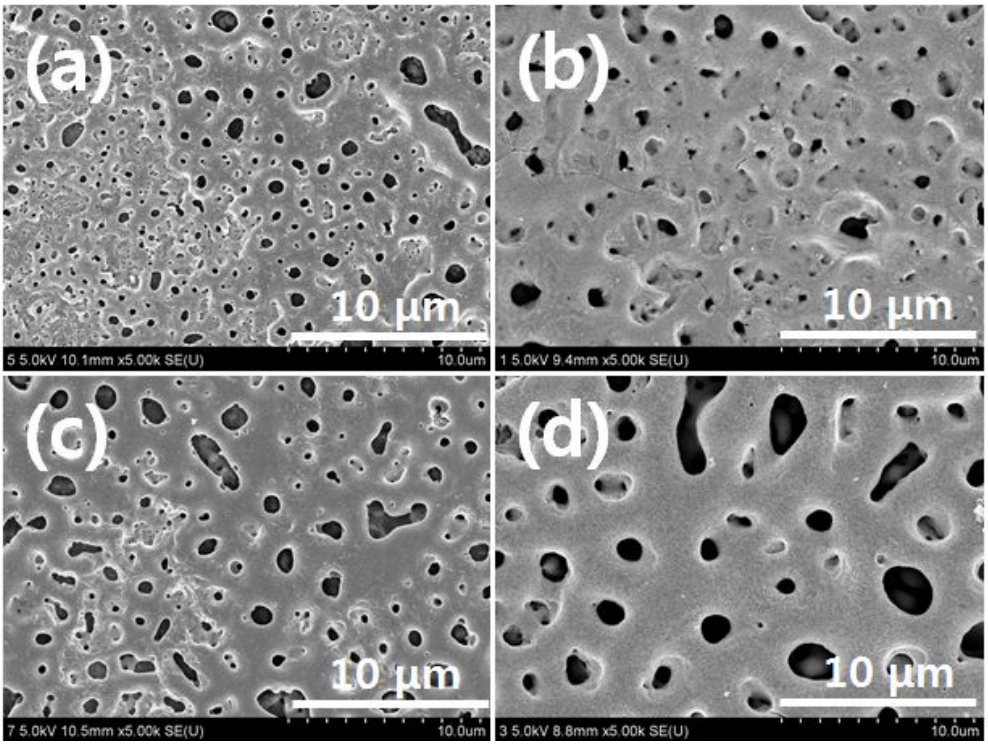

Fig. 9. FE-SEM images of micro-pore formed on Ti-35Ta-xNb alloys in 0.15 M calcium acetate monohydrate + 0.02 M calcium glycerophospate; (a) Ti-35Ta (b) NaOH treated Ti-35Ta (c) Ti-35Ta-10Nb (d) NaOH treated Ti-35Ta-10Nb.

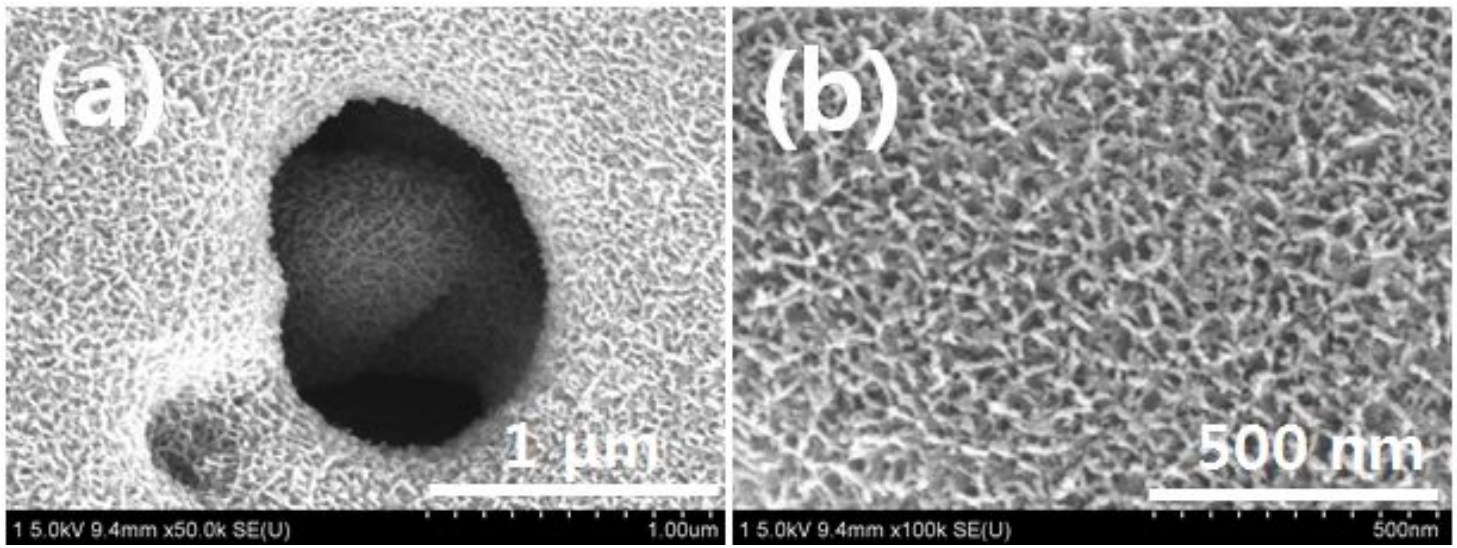

Fig. 10. FE-SEM images of NaOH treated micro-pore formed on Ti-35Ta alloy in 0.15 M calcium acetate monohydrate + 0.02 M Calcium glycerophospate.

The micro-pore size has influence on alloy production as shown in Fig. 9.

Fig. 11 shows the corelation between micro-pore formation time and applied voltages on Ti-35Ta-xNb alloys. The experiment is carried out for 3 min at the time of maintenance to 280V. The voltage increased proportionally up to 170V with high slope according to time, and then, variation of voltage with low slope is observed from 170V to 280V. It is thought that occurrences of spark discharge at 170 V is mainly appeared on surface due to insulation breakdown of the surface [60,61].

Fig. 12 shows The corelation between micro-pore formation time and current density on Ti-35Ta-xNb alloys. The first current density was kept continuously at 12 mA/cm^2, and then, current density was suddenly changed to 0 mA/cm^2 at 280 V due to the formation of barrier layer [62]. Especially, current density is changed irregularly at 0 mA/cm^2. It is confirmed that electrical unstability is appeared on the surface due to fornmation of micropores. The analysis of Fig. 11 and Fig. 12 is summarized as shown in Table 7. From the Table 7, in the process of forming micro-pore structured, the rate of forming barrier layer has been slow down with addition of Nb content. In previous paper, the dissolution rate of barrier layer is influenced by metallic phase [63]. As a result, the element of Nb has influence on alloy resistance and morphology of barrier layer.

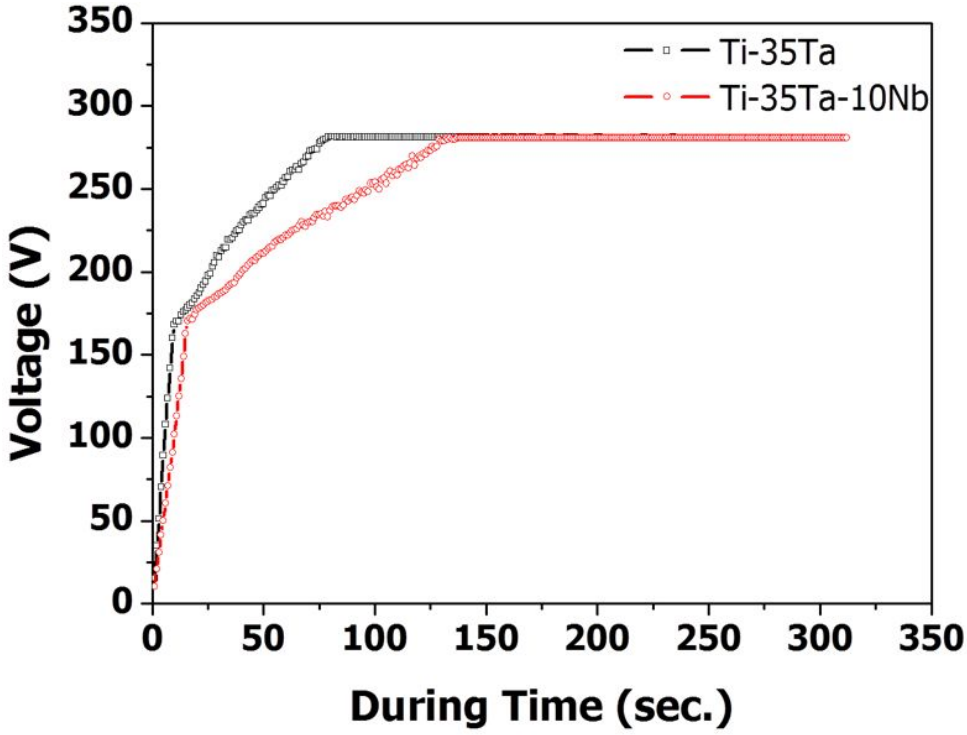

Fig. 11. The corelation between micro-pore formation time and voltage on Ti-35Ta-xNb alloys.

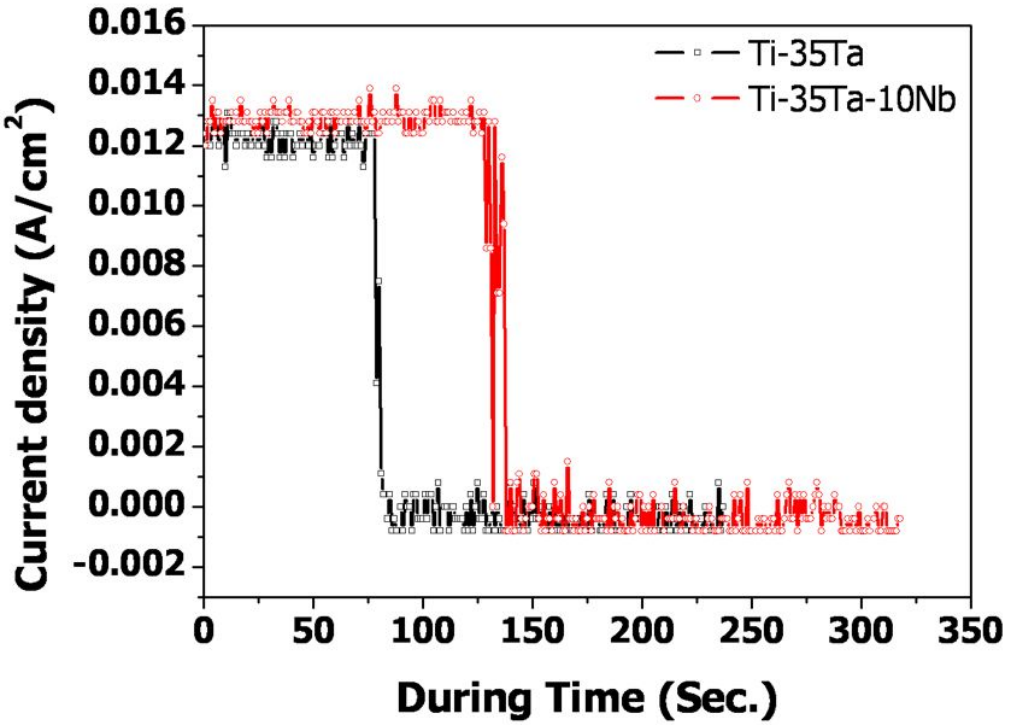

Fig. 12. The corelation between micro-pore formation time and current density on Ti-35Ta-xNb alloys.

Table 7 Voltage and current density value of Ti-35Ta-xNb alloys

	Inflection point		280 V	Pre stabilized		0 mA
	t (second)	Voltage	t (second)	t (second)	mA	t (second)
Ti-35Ta	11	170 V	78	78	12.4 mA	84
Ti-35Ta-10Nb	17	172 V	132	128	13.1 mA	138

4.3. Morphology of electrochemical deposition on Ti-35Ta-xNb alloys

Fig. 13 shows FE-SEM images of NaOH treated Ti-35Ta alloy in 2.5 mM $Ca(NO_3)_2 \cdot 4\ H_2O$ + 1.5 mM $NH_4H_2PO_4$. The Fig. 13(a) and Fig. 13(b) shows FE-SEM images of HA coatings on NaOH treated Ti-35Ta-xNb alloy. Fig. 13(c) and Fig. 13(d) shows FE-SEM images of high magnifications of HA coatings on NaOH treated Ti-35Ta-xNb alloy. Both HA coatings on Ti-35Ta and Ti-35Ta-10Nb alloy were formed on surface with general forms, especially, the HA shape of Ti-35Ta alloy is larger than that of Ti-35Ta-10Nb alloy. According to previous paper, the shape of HA is important role to decide the final shape and size[67]. And it is confirmed that the shape of HA has is affected by Nb content as shown in Fig 11 and Fig 12.

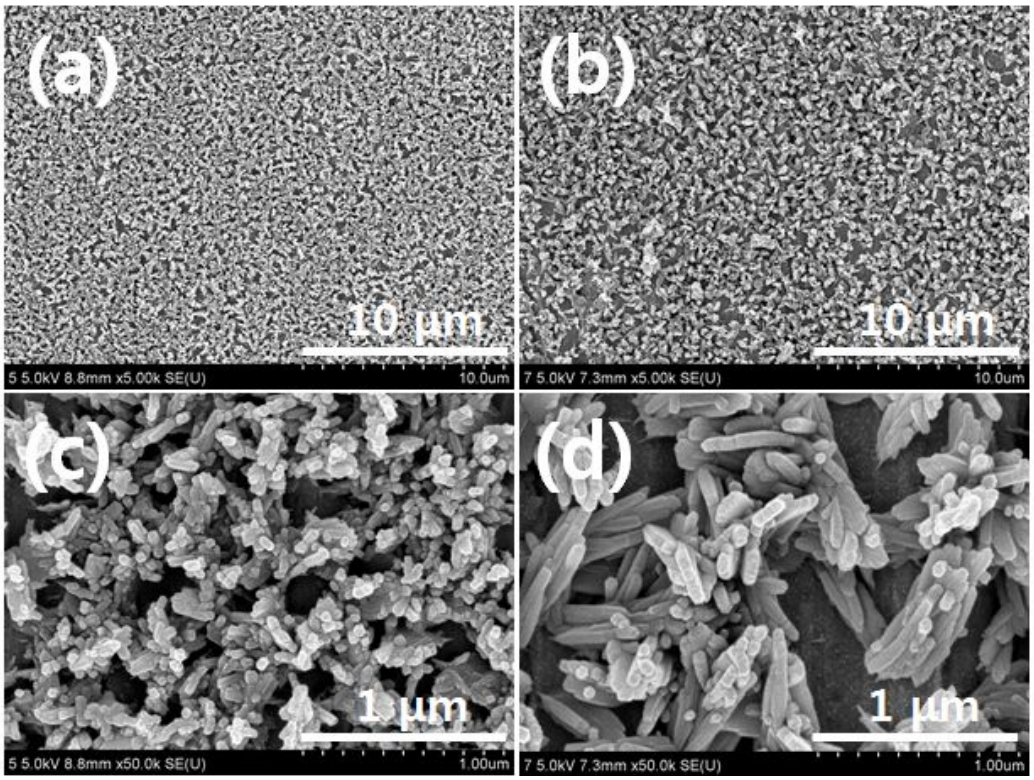

Fig. 13. FE-SEM images of NaOH treated Ti-35Ta alloy in 2.5 mM $Ca(NO_3)_2 \cdot 4\ H_2O$ + 1.5 mM $NH_4H_2PO_4$; (a) Ti-35Ta, (b) Ti-35Ta-10Nb, (c) high magnification of Ti-35Ta, (d) high magnification of Ti-35Ta-10Nb.

Fig. 14 shows the shapes of initial HA on Ti-35Ta-10Nb alloy in 2.5 mM $Ca(NO_3)_2 \cdot 4\ H_2O$ + 1.5 mM $NH_4H_2PO_4$. As shown in Fig. 14, the initial HA precipitation was formed in pore inside and outside. The formation of nucleation is leading to surface potential and temperature, which is evaluate to previous paper [68, 69].

Fig. 15 shows FE-SEM images of HA coating on NaOH treated micro-pore structured Ti-35Ta-xNb alloy in 2.5 mM $Ca(NO_3)_2 \cdot 4\ H_2O$ + 1.5 mM $NH_4H_2PO_4$. Fig. 15(a) shows flower-like HA shape, Fig. 15(c) shows flower-like HA shape of bi-phase. Also, the HA sizes of Ti-35Ta-10Nb alloy is bigger than that of Ti-35Ta alloy. It is confirmed that morphology of micro-pore depended on Nb content.

Fig. 16 shows FE-SEM images of HA coated and NaOH treated micro-pore structured Ti-35Ta-xNb alloy in 2.5 mM $Ca(NO_3)_2 \cdot 4\ H_2O$ + 1.5 mM $NH_4H_2PO_4$. The HA coating is formed on the whole surface, the HA size of Ti-35Ta-10Nb alloy shows the bigger than that of Ti-35Ta alloy. The deposition cycles increased, the size of precipitates increased [70]. The porous and HA doped surface of Ti-35Ta-xNb alloys has advantage of cell growth on the surface. Especially, HA coated layer can be applicated to dental implant [71].

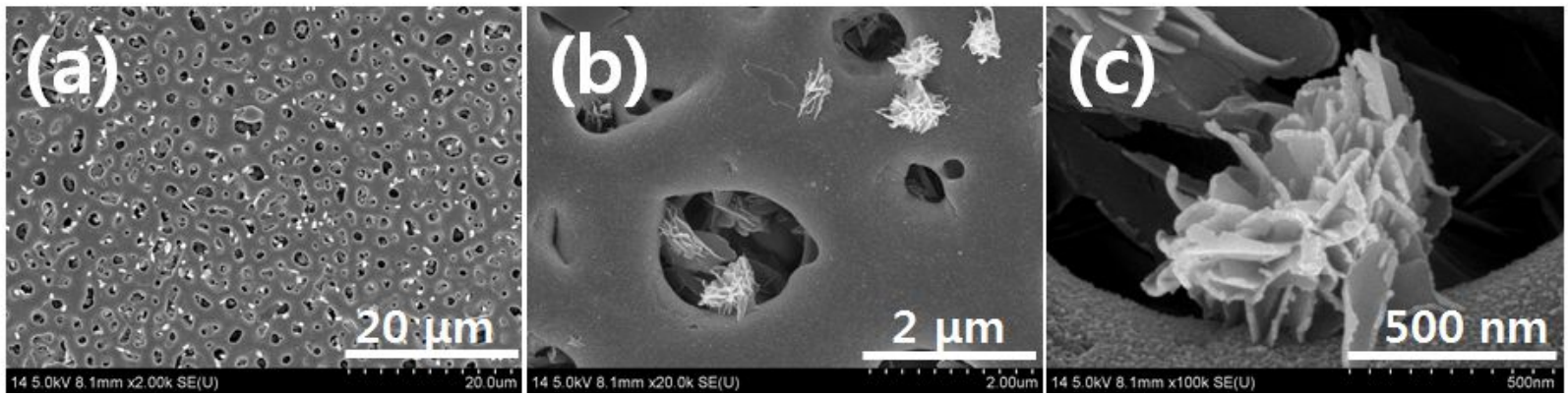

Fig. 14. FE-SEM images of initial step of HA crystal nucleation on NaOH treated Ti-35Ta-10Nb alloy in 2.5 mM $Ca(NO_3)_2 \cdot 4\ H_2O$ + 1.5 mM $NH_4H_2PO_4$ with 5 deposition cycles. (a) X 2,000, (b) 20,000 high magnification of (a), (c) 100,000 high magnification of (a)

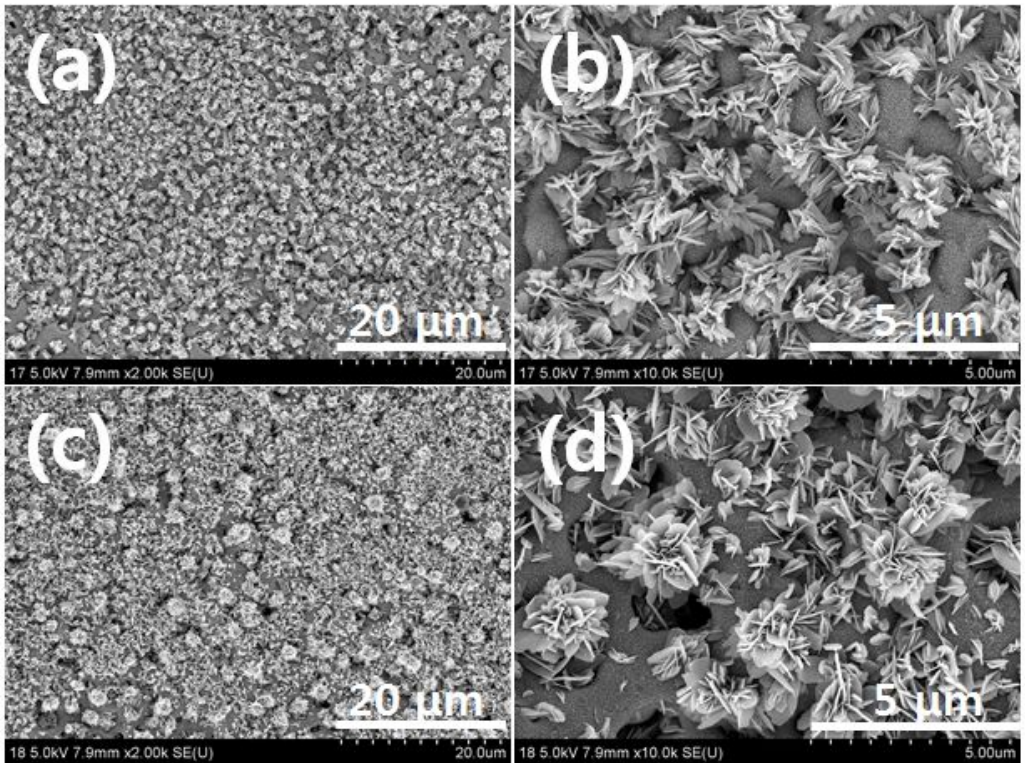

Fig. 15. FE-SEM images of HA coatings on NaOH treated micro-pore structured Ti-35Ta-xNb alloy in 2.5 mM $Ca(NO_3)_2 \cdot 4\ H_2O$ + 1.5 mM $NH_4H_2PO_4$ with 30 deposition cycles; (a) Ti-35Ta, (b) high magnification of Ti-35Ta, (c) Ti-35Ta-10Nb, (d) high magnification of Ti-35Ta-10Nb.

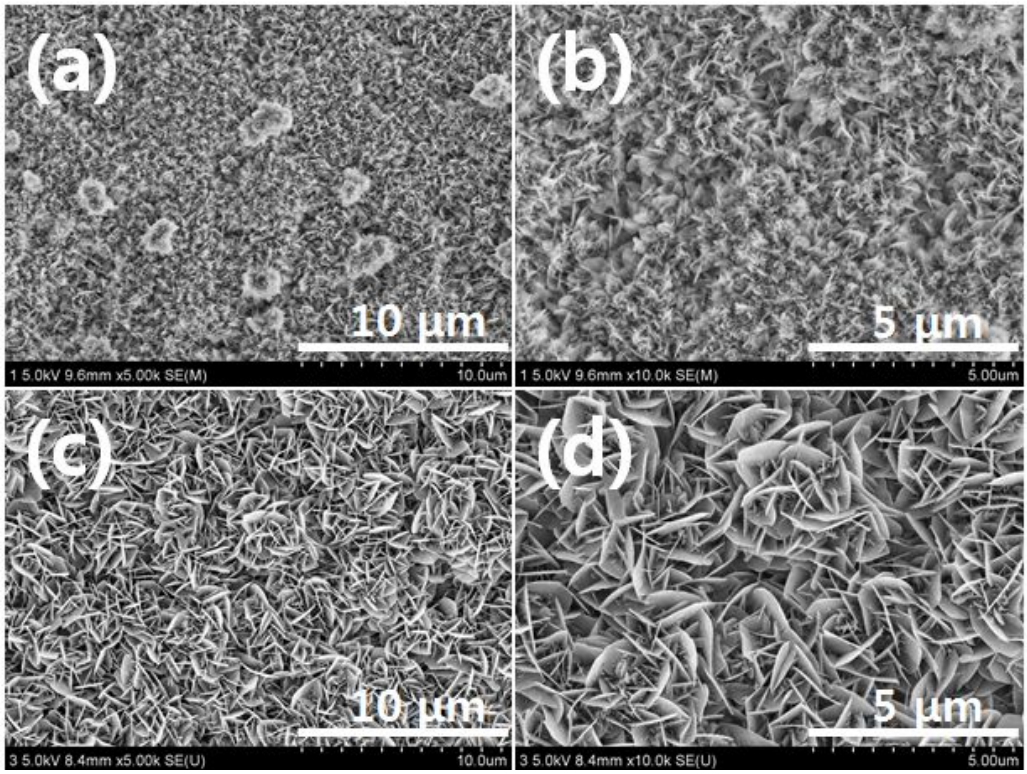

Fig. 16. FE-SEM images of HA coatings on NaOH treated micro-pore structured Ti-35Ta-xNb alloy in 2.5 mM $Ca(NO_3)_2 \cdot 4\ H_2O$ + 1.5 mM $NH_4H_2PO_4$ with 50 deposition cycles; (a) Ti-35Ta, (b) high magnification of Ti-35Ta, (c) Ti-35Ta-10Nb, (d) high magnification of Ti-35Ta-10Nb.

In order to detail discussion, Fig 17 and Fig 18 show corelation between voltage and current densities for Ti-35Ta-xNb alloys. From the figures show that the current density value of non treated Ti-35Ta-xNb alloys is lower than that of micro-pore structured Ti-35Ta-xNb alloys. Also, current density is changed with Nb content. The following equation shows the reduction and oxidation of cathode reaction [64].

$$2\ H_2PO_4^{2-} + 2\ e^- \rightarrow 2\ HPO_4^{2-} + H_2 \quad [1]$$

$$2\ H_2PO_4^{2-} + 2\ e^- \rightarrow 2PO_4^{3-} + H_2 \quad [2]$$

$$2\ H^+ + 2\ e^- \rightarrow H_2 \quad [3]$$

$$2\ H_2O + 2\ e^- \rightarrow H_2 + 2\ OH^- \quad [4]$$

It is result that chemical reaction take place in electrolyte solution and surface. The anodic oxide film to containing calcium and phosphorus is ionized to calcium ion(Ca^{2+}) and phosphorus ion(PO_4^{3-}) as initial cathode reaction. It's ions are reaction with electrolyte solution, calcium phosphate film is formed in surface. The ionized Ca^{2+} and PO_4^{3-} ions in oxide film is reduced $CaHPO_4$ and $H_2PO_4^{2-}$ and the reaction is repeated by 3 and 4. This reaction is carried out in anodized surface, HA is coated on anodized surface by additions 5 and 6.

$$Ca^{2+} + HPO_4^{2-} \rightarrow CaHPO_4 \quad [5]$$

$$PO_4^{3-} + H_2O \rightarrow H_2PO_4^{2-} + OH^- \quad [6]$$

$$10\ Ca^{2+} + 6\ PO_4^{3-} + 2\ OH^- \rightarrow Ca_{10}(PO_4)_6(OH)_2 \quad [7]$$

From Fig. 17, and Fig. 18, as the width of current density is increased, the HA size is increased. At the same voltage, resistance is inversed current

density. Therefore, the precipitation properties of surface treated alloy is depended on surface morphology and current density.

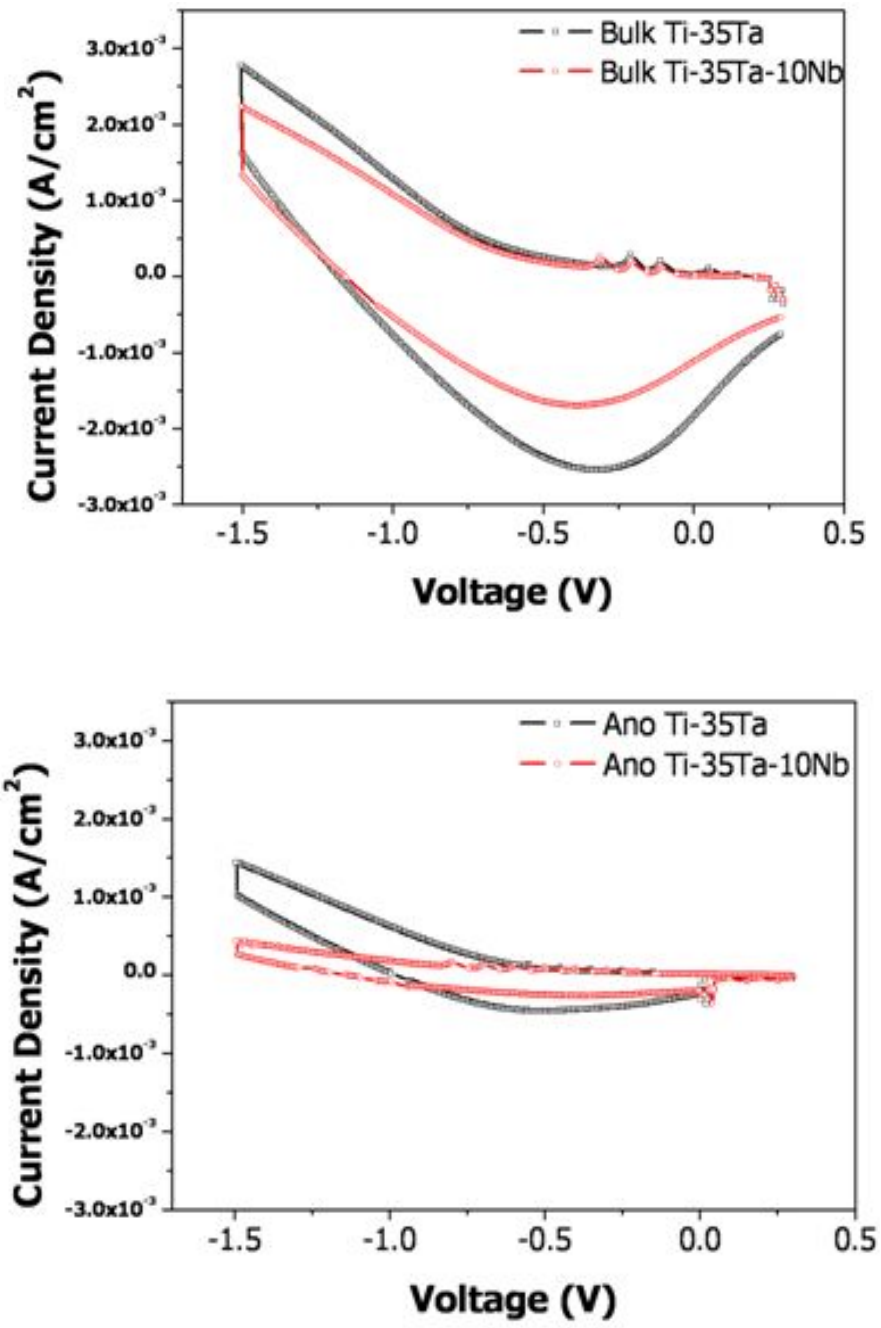

Fig. 17. The corelation between voltage and current densities on Ti-35Ta-xNb alloys; (a) HA coated on bulk Ti-35Ta-xNb, (b) HA coated on micro-pore structured Ti-35Ta-xNb.

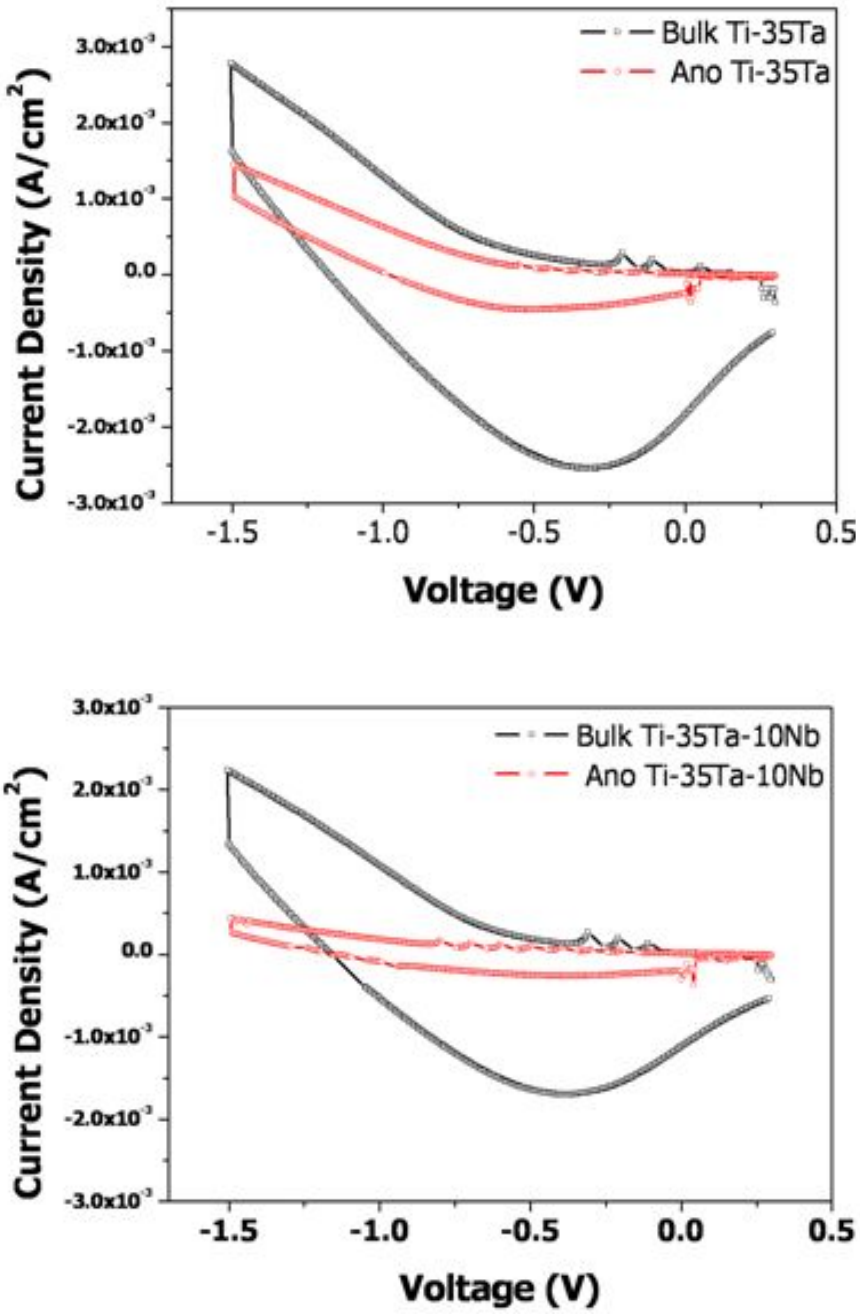

Fig. 18. The corelation between voltage and current densities on Ti-35Ta-xNb alloys.(a) HA coated Ti-35Ta, (b) HA coated Ti-35Ta-10Nb.

Table 8 Voltage value of bulk and anodize surface on Ti-35Ta-xNb alloy

		0.3 V			-1.5 V		
		start	end	| start - end |	start	end	| start - end |
Bulk	Ti-35Ta	-3.66×10^{-4}	-7.60×10^{-4}	3.94×10^{-4}	2.78×10^{-3}	1.61×10^{-3}	1.17×10^{-3}
	Ti-35Ta-10Nb	-3.05×10^{-4}	-5.36×10^{-4}	2.31×10^{-4}	2.23×10^{-3}	1.34×10^{-3}	8.9×10^{-4}
Anodized	Ti-35Ta	-3.44×10^{-4}	-1.45×10^{-4}	1.99×10^{-4}	1.44×10^{-3}	1.01×10^{-3}	4.3×10^{-4}
	Ti-35Ta-10Nb	-3.05×10^{-4}	-1.98×10^{-4}	1.07×10^{-4}	4.36×10^{-4}	2.64×10^{-4}	1.72×10^{-4}

4.5. Corrosion test

Fig. 19 shows the bulk surface and micro-pore structured Ti-35Ta-xNb alloys polarization curves after potentiodynamic test in 0.9 % NaCl solution at 36.5 ± 1 ℃. The results for E_{corr} (corrosion potential), I_{corr} (corrosion current density) and I_{300} (corrosion current density of oral environment at 300 mV)is shown in Table 9. These values were obtained from the polarization curves and Tafel plots using both the cathodic and anodic branches of the curves, respectively. From non treated and micro-pore treated Ti-35Ta-xNb alloys surface, the E_{corr} value of Ti-35Ta alloy is higher than that of Ti-35Ta-10Nb alloy. Also, the I_{corr} value of Ti-35Ta alloy is lower than that of Ti-35Ta-10Nb alloy. The polarization curves were shifted to left side with increasing Nb content and micro-pore structured Ti-35Ta-xNb alloys. It is confirmed that barrier layer and Nb_2O_5 film increased the corrosion resistance and it can be improved osseointegration [72].

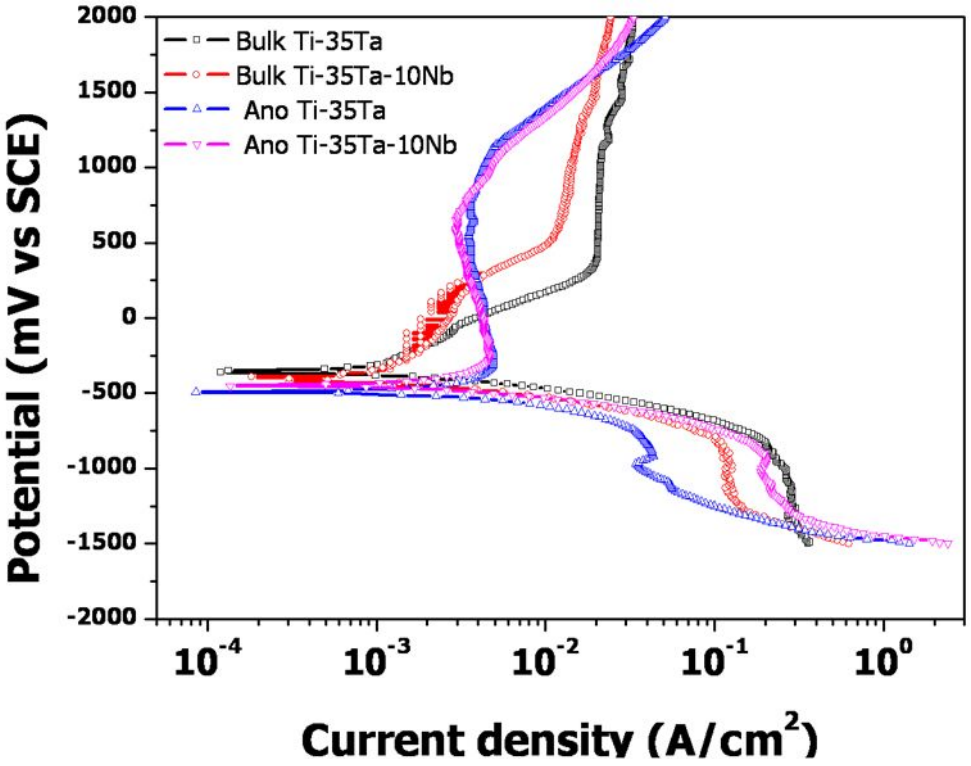

Fig. 19. Anodic polarization curves of Ti-35Ta-xNb alloys with surface treatment.

Table 9 E_{corr}, I_{corr} and I_{300mV} value of Ti-35Ta-xNb alloy

	Alloy	E_{corr}	I_{corr}	I_{300mV}
Bulk	Ti-35Ta	- 380 mV	8.63 X 10^{-7} A/cm^2	1.84 X 10^{-5} A/cm^2
	Ti-35Ta-10Nb	- 393 mV	8.47 X 10^{-7} A/cm^2	4.65 X 10^{-6} A/cm^2
Anodized	Ti-35Ta	- 479 mV	8.22 X 10^{-7} A/cm^2	3.69 X 10^{-6} A/cm^2
	Ti-35Ta-10Nb	- 429 mV	1.00 X 10^{-6} A/cm^2	3.45 X 10^{-6} A/cm^2

V. CONCLUSIONS

In this study, the surface characteristics of hydroxyapatite film on the micro-pore structured Ti-35Ta-xNb alloys by electrochemical deposition method were investigated by using various experimental instruments.

The results were as follows;

1. Microstructure of alloys were transformed form α" phase to β phase, and a needle-like to an equiaxed structure as Nb content increased.
2. The Ti-35Ta and Ti-35Ta-10Nb alloy showed only α"+ β phase and crystal structure from XRD analysis.
3. The number of micro-pore increased as Nb content increased and the micro-pore size increased as voltage increased.
4. Nano network structure was formed on NaOH treated Ti-35Ta-xNb alloys.
5. HA size of Ti-35Ta-10Nb alloy is bigger than that of Ti-35Ta alloy.
6. Flower-like HA shape showed on the Ti-35Ta alloy surface, whereas, the bi-phase flower-like HA shape showed on the Ti-35Ta-10Nb alloy. HA size on the Ti-35Ta-10Nb alloy is bigger than that of Ti-35Ta alloy.
7. Corrosion resistance of Ti-35Ta-xNb alloys increased as Nb content increased.

- Reference -

1. H. J. Rack, J. I. Qazi, Mater. Sci. Eng. C 26 (2006) 1269-1277.
2. R. Brånemark, P. I Brånemark, B. Rydevik, R. R. Myers, J. Rehabil. Res. Dev. 38 (2001) 175-181.
3. T. I. Kim, J. H. Han, I. S. Lee, K. H. Lee, M. C. Shin, B. B. Choi, BioMed. Mater. Eng. 7 (1997) 253-263.
4. D. Kuroda, M. Niinomi, M. Morinaga, Y. Kato, T. Yashiro, Mater. Sci. Eng. A243 (1998) 244-249.
5. J. O. C. Silva, E. A. S. Paiva, L. V. Modolo, C. C. Nascentes, M. G. C. Franca, Environ. Exp. B. 95 (2013) 41-49.
6. K. Kyzioł., Ł. Kaczmarek, G. Brzezinka, A. Kyzioł. Chem. Eng. J. 240 (2014) 516-526.
7. D. M. Gordin, T. Gloriant, Gh. Nemtoi, R. Chelariu, N. Aelenei, A. Guillou, D. Ansel, Mater. Letters 59 (2005) 2936-2941.
8. R. Palanivelu, S. Kalainathan, A. Ruban Kumar, Ceramics International 40 (2014) 7745-7751.
9. Y. H. Jeong, H. C. Choe, W. A. Brantley, Appl. Surf. Sci. 258 (2012) 2129-2136.
10. H. Wang, F. Liu, Y. Zhang, F. Wang, Surf. Coat. Technol. 206 (2012) 4054-4059.
11. C. X. Wang, M. Wang, X. Zhou, Biomaterials 24 (2003) 3069-3077.
12. C. Vasilescu, P. Drob, E. Vasilescu, I. Demetrescu, D. Ionita, M. Prodana, S. I. Drob, Corrosion Science 53 (2011) 992-999.
13. A. Bigi, M. Fini, B. Bracci, E. Boanini, P. Torricelli, G. Giavaresi, N. N. Aldini, A. Facchini, F. Sbaiz, R. Giardino, Biomaterials 29 (2008) 1730-1736.
14. K. Lee, Y. H. Jeong, W. A. Brantley, H. C. Choe, Thin Solid Films 546 (2013) 185-188.

15. H. H. Huang, C. P. Wue, Y. S. Sun, W. E. Yang, T. H. Lee, J. Alloys. Compd. 615 (2014) S648-S654.
16. P. Malmberg, H. Nygren, Proteomics 8 (2008) 3755-3762.
17. M. V. Regı, J. M. G. Calbet, Progress in Solid State Chemistry 32 (2004) 1-31.
18. R. Narayanan, S. K. Seshadri, T. Y. Kwon, K. H. Kim, J. Biomed. Mater. Res. B 85 (2007) 279-299.
19. D. B. McGregor, R. A. Baan, C. Partensky, J. M. Rice, J. D. Wibourn, Eur. J. Cancer. 36 (2000) 307-313.
20. E. W. Collings, The physical matallurgy of titanium alloys, American Society for Metals (1984) pp.3-5.
21. M. Long, H. J. Rack, Biomaterials 19 (1998) 1621-1639.
22. Y. Okazaki, Y. Ito, K. Kyo, T. Tateisi, Mater. Sci. Eng. A213 (1996) 138-147.
23. N. E. Paton, J. C. Williams, Effect of hydrogen on titanium and its alloys, American Society for Metals. (1974) 409-432.
24. M. J. Donachie, Titanium and Titanium Alloys-Source Book, American Society for Metals (1982).
25. S. H. Jang, H. C. Choe, Y. M. Ko, W. A. Brantely, Thin Solid Films 517 (2009) 5038-5043.
26. M. McCrajeb, J. Prosthodont 8 (1999) 40-43.
27. J. K. Breme, V. Biehl, W. Schults, B. D'Hoedt, K. Donath, Biomaterials 14 (1993) 887-892.
28. V. D. Cojocatu, D. Raducanu, T. Gloriant, I. Cinca, J. Met. 64 (2012) 572-581.
29. J. I. Qazi, B. Marquardt, H, J. Rack, J. Met. 56 (2004) 49-51.
30. P. N. Kumta, C. Sfeir, D-H. Lee, D. Choi. Acta Biomater. 1 (2005) 65-83.
31. M. Geetha, A. K. Singh, R. Asokamani, A. K. Gogia, Progress in Mater. Sci. 54 (2009) 397-425.
32. S. Winter, D. Velten, F. Aubertin, Metallic Biometerial Interfaces,

Willy-VCH, (2008) 5.

33. S. S. Mehdi, M. T. Khorasani, D. K. Ehsan, J. Ahmad, Acta Biomaterialia 9 (2013) 7591-7621.

34. A. Märten, P. Fratzl, O. Paris, P. Zaslansky, Biomaterials 31 (2010) 5479-5490.

35. D. Z. Chen, C. Y. Tang, K. C. Chan, C. P. Tsui, P. H. F. Yu, M. C. P. Leung, P. S. Uskokovic, Compos. Sci. Technol. 67 (2007) 1617-1626.

36. P. O'Hare, B. J. Meenan, G. A. Burke, G. Byrne, D. Dowling, J. A. Hunt, Biomaterials 31 (2010) 515-522.

37. E. Foresti, J. Inorg. Biochem. 15 (1981) 317-327.

38. A. Biesiekierski, J. Wang, M. A-H. Gepreel, C. Wen, Acta Biomaterialia 8 (2012) 1661-.1669.

39. T. Hanawa, Japanese Dental Science Review 46 (2010) 93-101.

40. H. shizawa, M. Ogino, J. Biomed. Mater. Res. 29 (1995) 1071-1079.

41. Y. Han, S. H. Hong, K. W. Xu, Surf. Coat. Technol. 168 (2003) 249-258.

42. F. Liu, F. P. Wang, T. Shimizu, K. Igarashi, L. C. Zhao, Surf. Coat. Technol. 199 (2005) 220-224.

43. W. Ma, J. H. Wei, Y. Z. Li, X. M. Wang, H. Y. Shi, S. Tsutsumi, et al. J. Biomed. Mater. Res. B 86B (2008) 162-169.

44. S. Ban, S. Maruno, N. Arimoto, A. Harada, J. Hasegawa, J. Biomed. Mater. Res. 36 (1997) 9-15.

45. A. Yuda, S. Ban, Y. Izumi, Dent. Mater. J. 24 (2005) 588-595.

46. K. Kuroda, M. Moriyama, R. Ichino, M. Okido, A. Seki, Mater. Trans. 49 (2008) 1434-1440.

47. M. Hosaka, Y. Shibata, T. Miyazaki, J. Biomed. Mater. Res. B 78B (2006) 237-242.

48. Y. Tanaka, E. Kobayashi, S. Hiromoto, K. Asami, H. Imai, T. Hanawa, J. Mater. Sci. Mater. Med. 18 (2007) 797-806.

49. R. Narayanan, S. K. Seshadri, T. Y. Kwon, K. H. Kim, J. Biomed. Mater. Res. B 85 (2007) 279-299.

50. T. Hayakawa, M. Kawasaki, G. H. Takaoka, J. Ceram. Soc. Jpn. 116

(2008) 68-73.
51. R. Narayanan, S. K. Seshadri, T. Y. Kwon, K. H. Kim, Scr. Mater. 56 (2007) 229-232.
52. R. Narayanan, T. Y. Kwon, K. H. Kim, J. Biomed. Mater. Res. B 85B (2008) 231-239.
53. R. Narayanan, T. Y. Kwon, K. H. Kim, Mater. Sci. Eng. C 28 (2008) 1265-1270.
54. R. Narayanan, S. Y. Kim, T. Y. Kwon, K. H. Kim, J. Biomed. Mater. Res. A 87A (2008) 1053-1060.
55. X. W. Meng, T. Y. Kwon, K. H. Kim, Dent. Mater. J. 27 (2008) 666-671.
56. T. Ozaki, H. Matsumoto, S. Watanabe, S. Hanada, Mater. Trans. 45 (2004) 2776-2779.
57. Y. L. Hao, S. J. Li, S. Y. Sun, C. Y. Zheng, R. Yang, Acta Biomater. 3 (2007) 277-286.
58. M. A. Hady, K. Hinoshita, M. Morinaga, Scr. Mater. 55 (2006) 477-480.
59. S. Winter, D. Velten, F. Aubertin, Metallic Biometerial Interfaces, Willy-VCH, (2008) 5.
60. A. Kaminska, A. Sionkowska, Polym. Degrad. Stabil. 51 (1996) 19-26.
61. A. L. Bacatella, H. S. Gadiyar, A. L. Sutton J. Electrochem. Soc 128 (1981) 1431-1537.
62. Y. Mizukoshi, N. Ohtsu, N. Masahashi, Appl. Surf. Sci. 283 (2013) 1018 - 1023.
63. T. E. Park, H. C. Choe, W. A. Brantley, Surf. Coat. Technol. 235 (2013) 706-713.
64. B. H. Lee, Y. D. Kim, J. H. Shin, K. H. Lee, J. Biomed. Mater. Res. 61 (2002) 466-473.
65. T. Kokubo, H. M. Kim, M. Kawashita, Biometerials 24 (2003) 2161-2175.
66. N. Moronuki, M. Nishio, Y. Tanaka, Procedia Eng. 19 (2011) 276 -281.
67. E. Mohseni, E. Zalnezhad, A. R. Bushroa, Int. J. Adhesion Adhesives 48 (2014) 238-257.
68. M. Lindgren, M. Astrand, U. Wiklund, H. Engqvist, J. Mater. Sci.

Mater. Med. 20 (2009) 1401-1408.

69. H. Qu, M. Wei, J. Biomed. Mater. Res. 87B (2008) 204-212.

70. C. I. Jo, Y. H. Jeong, H. C. Choe, W. A. Brantley, Thin Solid Films 549 (2013) 135-140.

71. M. Lilja, U. Butt, Z. Shen, D. Bjoorn, Appl. Surf. Sci. 284 (2013) 1-6.

72. V. S. Saji, H. C. Choe, W. A. Brantely, Acta Biomater. 5 (2009) 2303-2310.

감사의 글

학교공지사항의 글을 보면서 찾아온 게 엊그제 같은데 벌써 석사과정의 마지막을 앞두고 본 논문을 작성하는 시기가 찾아오게 되었습니다. 그동안 치과재료학 교실에서 많은 것을 배우고 경험하였고 이러한 바탕이 앞으로 살아가는데 도움이 될 것이라고 믿어 의심치 않습니다. 짧다면 짧고 길다면 긴 석사과정을 무사히 마칠 수 있게 도움을 주신 분들에게 이 글에서나마 감사의 글을 전하고 싶습니다.

우선 지금도 많이 부족하지만 항상 많은 것을 가르쳐주셨고 경험할 수 있게 도와주시고 지원해주신 지도교수 최한철 교수님의 은혜를 잊지 않겠습니다. 특히 교수님께서 강조하신 행실의 중요성과 예의의 중요성을 항상 기억하고 실천하는 제자가 되도록 하겠습니다. 또한 그동안 실험분석을 할 때 기꺼이 도움을 주셨고 이번 논문심사에도 애정 어린 조언을 주시고 특히 저의 처음 해외로 나간 한 회에서 무사히 임무를 완수할 수 있도록 도움을 주신 김병훈 교수님과 저희 실험실의 분석에 많은 도움을 주시고 이번 논문에 관심을 가져주신 안상건 교수님께 감사의 글을 남기고 싶습니다.

이번 논문을 작성하는데 많은 조언과 관심을 가진 이강 박사님께 감사드리며 그동안 박사님께서 가르쳐주신 지식과 늦게 퇴근할 때마다 저에게 해주신 말씀은 지금도 좋은 기억으로 저에게 남아있습니다. 맨 처음 아무것도 모를 때 들어왔는데 상냥하게 저를 대해주신 병학이형과 은주누나, 감사합니다. 그리고 먼저 졸업하여 자리를 잡아 모르는 사항이 있어 연락을 할 때마다 친절하게 답변을 주었던 성환이형과 현주형, 그리고 은실이에게 감사의 글을 남기고 싶고 자주 연락할 수 있었으면 좋겠습니다. 부족한 나의 후임으로 들어와 알려주면 스펀지처럼 금방 흡수하여 실험과 일처리를 잘했었고 지금도 잘하고 있고 앞으로도 잘할 인섭이, 네가 있어서 석사과정을 즐겁게 그리고 무사히 끝마칠 수 있어서 고맙다. 그리고 늦다면 늦은 나이에 쉽지않은 선택을 하여 별이 보일때에만 퇴근을 하시고 최선을 다하는 자세로 임하시고 김정재 박사님, 제가 이따금씩 고민을 이야기 할 때마다 단 한번도 건성으로 대답을 해보신적이 없으시고 진심어린

조언을 해주시는 모습에 많이 배웠습니다. 그리고 이번에 들어온 지 몇 개월이 안됐지만 항상 밝고 긍정적이고 밝은 실험실 분위기를 만드는 선영이, 일을 배울 때도 열의있게 배우는 그 모습을 보고 많이 배웠고 앞으로도 잘할것이라 믿어 의심치 않는다. 그리고 서로 안지는 오래되었지만 치과재료학교실에 자주 오면서 최근에 많이 친해진 정인이, 1년 동안 손미경 교수님이 없는 기간에 우리 교수님에게 많은 것을 배우게 될 것이고 분명히 많은 도움이 될거야.

끝으로 항상 묵묵히 저를 지켜봐주시고 항상 제 편인 부모님, 효도다운 효도도 제대로 못해드려도 괜찮다며 말씀해주시는 부모님, 제가 이 석사를 방황하지 않고 끝낼 수 있게 해준 이유이자 원동력이었습니다. 그리고 자신의 꿈을 위해 오늘도 즐겁고 열심히 생활하고 있는 내 하나뿐인 동생아, 보기 좋다. 그리고 가진거라고는 몸밖에 없는 나의 옆에 있어주고 힘들 때마다 나에게 힘을 준 여자친구, 내옆에 있어서 항상 고맙고 고맙다. 그 외에 석사과정에서 만난 소중한 모든 인연들에게 감사하다는 말을 남기고 글을 마치겠습니다.

2014.02.
조채익 올림

저작물 이용 허락서

학 과	광기술공학과 (광응용공학전공)	학 번	20137155	과 정	석사
성 명	한글: 조 채 익 한문 : 趙 采 翼 영문 : Jo Chae-Ik				
주 소	광주광역시 광산구 월계동 건영아파트 105동 1104호				
연락처	E-MAIL : blackjuice88@nate.com				
논문제목	한글 : 전기화학적 석출법으로 마이크로 포어구조를 형성한 Ti-35Ta-xNb 합금의 수산화인회석 피막의 표면 특성 영어 : Surface Characteristics of Hydroxyapatite Film on the Micro-pore Structured Ti-35Ta-xNb Alloys by Electrochemical Deposition Method.				

본인이 저작한 위의 저작물에 대하여 다음과 같은 조건아래 조선대학교가 저작물을 이용할 수 있도록 허락하고 동의합니다.

- 다 음 -

1. 저작물의 DB구축 및 인터넷을 포함한 정보통신망에의 공개를 위한 저작물의 복제, 기억장치에의 저장, 전송 등을 허락함
2. 위의 목적을 위하여 필요한 범위 내에서의 편집·형식상의 변경을 허락함. 다만, 저작물의 내용변경은 금지함.
3. 배포·전송된 저작물의 영리적 목적을 위한 복제, 저장, 전송 등은 금지함.
4. 저작물에 대한 이용기간은 5년으로 하고, 기간종료 3개월 이내에 별도의 의사표시가 없을 경우에는 저작물의 이용기간을 계속 연장함.
5. 해당 저작물의 저작권을 타인에게 양도하거나 또는 출판을 허락을 하였을 경우에는 1개월 이내에 대학에 이를 통보함.
6. 조선대학교는 저작물의 이용허락 이후 해당 저작물로 인하여 발생하는 타인에 의한 권리 침해에 대하여 일체의 법적 책임을 지지 않음
7. 소속대학의 협정기관에 저작물의 제공 및 인터넷 등 정보통신망을 이용한 저작물의 전송·출력을 허락함.

동의여부 : 동의(O) 반대( )

2015 년 02 월 25 일

저작자: 조 채 익 (서명 또는 인)

조선대학교 총장 귀하